THE BOUNDARY LAYER OVER A LONG BLUNT FLAT PLATE IN HYPERSONIC FLOW

by

NORBERT ANDREW DURANDO

SUBMITTED IN PARTIAL FULFILLMENT
OF THE REQUIREMENTS FOR THE
DEGREES OF
BACHELOR OF SCIENCE AND MASTER OF SCIENCE

at the

MASSACHUSETTS INSTITUTE OF TECHNOLOGY
September, 1961

Signature of Author_____
Department of Aeronautics and
Astronautics, September, 1961

Certified by_____
Thesis Supervisor

Accepted by_____
Chairman, Departmental
Graduate Committee

THE BOUNDARY LAYER OVER A LONG BLUNT FLAT PLATE IN HYPERSONIC FLOW

by

NORBERT ANDREW DURANDO

Submitted to the Department of Aeronautics and Astronautics on August 21, 1961 in partial fulfillment of the requirements for the degrees of Bachelor of Science and Master of Science.

ABSTRACT

The contribution of the boundary layer to the surface pressure on a long blunt flat plate is calculated for a free stream Mach number of 7.6 and a free stream stagnation Reynolds number of 95,700. The plate is assumed to be insulated and the Prandtl number assumed to be unity. Non-isentropic effects produced by the curved bow shock are included by allowing for a variable stagnation pressure at the edge of the boundary layer. Isentropic calculations are carried out first in order to provide asymptotes which non-isentropic results should approach near the leading edge and far from the leading edge. The stagnation pressure is then allowed to vary along the edge of the boundary layer, but as a simplifying approximation the static pressure is at first assumed to be constant along the plate. Finally, the complete problem with variable static and stagnation pressures is solved. Integral methods are used throughout, in conjunction with Thwaites' approximate universal relationships.

Thesis Supervisor: Morton Finston

Title: Associate Professor of Aeronautics and Astronautics

ACKNOWLEDGEMENTS

The author wishes to express his gratitude to Professor Morton Finston for his helpful suggestions during the preparation of this paper. To Mr. Jacques A. Hill, thanks for his guidance during the earlier stages of this work. To Mrs. Edith Sandy, the author's appreciation for her invaluable help in the programming of the instructions for the IBM 709 computer of the M.I.T. Computation Center. Thanks are extended to Miss Theodate Coughlin for her competent handling of an unenviable typing task, and to the staffs of the M.I.T. Aerophysics Laboratory and Computation Center for the use of their facilities in the preparation of the thesis.

TABLE OF CONTENTS

LIST OF SYMBOLS

a speed of sound

a' definition in Fig. 15

l Thwaites parameter

m Thwaites parameter

p pressure

q_w heat flow per unit time at the surface

u velocity in the x direction

v velocity in the y direction

x coordinate along the plate

y coordinate normal to the plate

x_1 Cartesian coordinate

y_1 Cartesian coordinate

B $\dfrac{2 l_s K_s^2}{Re_{D_2}} \dfrac{1}{M_1^2} \dfrac{p_{o_2}}{p_1} \dfrac{T_1}{T_{o_2}} = constant$

C constant defined in Eq. (4.9)

C' constant defined in Eq. (5.11a)

D diameter of semicircular leading edge or plate thickness

G constant defined in Eq. (5.8c)

H Thwaites parameter

J constant defined in Eq. (5.8a)

J' $\dfrac{J}{3.2}$

K $\dfrac{\delta - \delta^*}{\theta}$

L_s Thwaites parameter

M Mach number

Pr Prandtl number

R Gas constant

Re Reynolds number

S incompressible coordinate in the y direction defined by

$$S = \int_0^y \frac{T_e}{T}\, dy$$

T temperature

U_e x velocity at the edge of the boundary layer

V_e y velocity at the edge of the boundary layer

β constant of proportionality in initial Mach number distribution

γ c_p/c_v ratio of specific heats

δ boundary layer thickness

δ_{det} see Fig. 15

δ^* displacement thickness

ϵ_s see Fig. 15

ζ $(Y_1/K_S D)^2$

η $(Y_1/D)^2$

θ momentum thickness

μ coefficient of viscosity

μ_1 see Fig. 15

ξ non-dimensional coordinate along the plate

ρ density

ϕ local shock inclination angle

CHAPTER 1

INTRODUCTION

1.1 Statement of Problem

When a blunt body travels through the atmosphere at a high Mach number, the proximity of the bow shock to the surface of the vehicle suggests that the boundary layer may have an important effect upon the surface pressure distribution. Inviscid theories are usually modified to allow for the presence of a boundary layer by modifying the actual body thickness to include some measure of the boundary layer thickness, and applying the inviscid velocity tangency condition at this modified surface rather than at the actual body surface. This procedure must be iterative because some kind of a surface pressure distribution is necessary in order to calculate the boundary layer thickness in the first place. One may thus proceed as follows: Calculate a surface pressure distribution using an inviscid theory, such as the blast wave analogy or the method of characteristics. With this pressure distribution, calculate some measure of the boundary layer thickness - in particular, the displacement thickness. Modify the inviscid pressure distri-

bution by assuming the body thickness has been increased by the displacement thickness. The simplest possible correction to the inviscid pressure distribution may be calculated by assuming a Prandtl-Meyer expansion about the modified body shape, with a local slope equal to the local slope of the boundary layer thickness. This simple procedure will be used in this paper. It is justified as long as the body under consideration has a smoothly varying slope. With the corrected pressure distribution the boundary layer displacement thickness may be recalculated, and this iterative procedure may be continued until the displacement thickness converges to some final distribution.

If in addition to a blunt nose the body has a large length-to-thickness ratio, the effect of the curved bow shock on the boundary layer becomes significant. Streamlines intersecting the shock at different points undergo different entropy losses and consequently different stagnation pressure drops. The curved shock will therefore cause the stagnation pressure to vary within the flow field. As the boundary layer thickens along the surface, it will grow into this region of variable stagnation pressure, which will affect the velocity and static temperature at the edge of the boundary layer.

The problem to be solved is the calculation of the boundary layer influence on the inviscid pressure distri-

bution over a blunt body of large length-to-thickness ratio, allowing for the effect of variable stagnation conditions along the edge of the boundary layer. The approach developed is applicable to two-dimensional blunt bodies of general shape, provided their slopes vary smoothly. However, the solution is carried out in detail for the particular case of a flat plate with a semicircular leading edge, placed at zero angle of attack in a stream flowing at a Mach number of 7.6. Experimental and semi-empirical relationships are used to calculate the static pressure distribution along the plate. The calculation of the pressure correction produced by the boundary layer will then indicate how much of this experimental surface pressure has been contributed by the boundary layer. This calculation will therefore show by how much a pressure distribution calculated from inviscid theory will differ from the actual pressure distribution.

1.2 Assumptions and Pertinent Experimental Results

The static pressure distribution along the plate has been obtained from two sources: Along the semicircular leading edge from the stagnation point to the shoulder, data obtained from tests conducted at the Aerophysics Laboratory of the Massachusetts Institute of Technology

are used. Downstream of the shoulder, a blast wave formula modified for better agreement with experimental results is used. This formula has been presented by Love in Ref. 1. The constants in the pressure formula have been adjusted to match the experimental results at the shoulder.

The free stream Reynolds number is high enough to permit two important assumptions:

1. The boundary layer near the leading edge is much thinner than the shock layer.
2. The effect of entropy gradients on the boundary layer may be estimated by allowing for variable stagnation edge conditions, disregarding the inviscid velocity gradient normal to the surface (see Ref. 2).

In addition, a hyperbolic shock shape is assumed, with a standoff distance obtained from semi-empirical results presented by Love in Ref. 3. Three simplifying assumptions are also made: The Prandtl number is unity, the heat transfer at the surface is zero, and the air is treated as a perfect gas.

1.3 General Approach

In Ref. 4 Hammitt has obtained the pressure influence of a boundary layer with variable stagnation edge conditions

for the case of a blunt flat plate. His solution involves the assumption of a one-parameter sixth-order polynomial to represent the velocity distribution within the boundary layer. The simpler, integral approach will be used in this paper, in conjunction with Thwaites'[5] approximate relationships between the first and second derivatives of the velocity at the surface, which hold for a one-parameter family of solutions.

In the subsequent chapters the solution to the pressure influence of the boundary layer is given for conditions of increasing difficulty. In the first place, the entropy gradient produced by the curved shock is neglected. This is done to provide limits which the non-isentropic solution should approach near the leading edge and very far from the leading edge, as well as to suggest the possibility of representing the actual blunt plate with variable static pressure by a constant pressure plate. Secondly, the assumption of isentropic flow is relaxed and the edge stagnation pressure allowed to vary. As a simplifying approximation, however, the static pressure is assumed to be constant along the plate. Finally, the complete problem with variable static and stagnation pressures is solved.

CHAPTER 2

ISENTROPIC RESULTS

2.1 Asymptotic Approximations

Near the leading edge of the plate the boundary layer is very thin and the mass flow in the boundary layer will therefore be small. This small amount of mass will be bounded upstream of the shock by streamlines which lie close together. These streamlines will all go through an essentially normal shock and consequently undergo approximately the same entropy change. Consequently, the boundary layer edge conditions near the leading edge of the plate may be considered to be isentropic, with a stagnation pressure equal to the stagnation pressure at the nose. Very far from the leading edge, the boundary layer is thick, and streamlines bounding its mass flow will intersect the shock at points where it is essentially a Mach line. Boundary layer edge conditions will again be essentially isentropic, but in this case the stagnation pressure will be equal to the free stream stagnation pressure. Furthermore, as the bow shock approaches a Mach line, the static

pressure will approach the free stream static pressure. When variable stagnation edge conditions are allowed for, it follows then that they will be bracketed by isentropic results near the leading edge and far downstream. Because of this asymptotic behavior of the non-isentropic edge conditions, it is important to consider the isentropic problem.

The above discussion suggests that the following isentropic solutions should be examined:

1) An isentropic blunt plate (V.P.-C.E.) whose stagnation pressure corresponds everywhere to the stagnation pressure at the nose.
2) An isentropic sharp plate (S.P.) whose bow shock is simply a Mach line, and whose stagnation and static pressures are everywhere equal to the free stream values.

In addition, it will be found that the static pressure distribution over the isentropic blunt plate (V.P.-C.E.) soon becomes constant and equal to the free stream static pressure. This fact suggests the introduction of a third isentropic approximation. For this case, the static pressure is assumed to be everywhere equal to the free stream static pressure, while the stagnation pressure is everywhere equal to that at the nose. This last approximation will be referred to as the "isentropic-constant pressure blunt plate" (C.P.-C.E.).

2.2 Pressure Distribution

As stated in Chapter 1, direct wind tunnel results at a free stream Mach number of 7.6 are used to obtain the static pressure distribution about the semicircular leading edge. Downstream of the shoulder, the following formula, given by Love in Ref. (1) is used to compute the pressure distribution:

$$\frac{p_e}{p_{o_2}} = \left[\frac{1}{1+\left(\frac{x-x_s}{D}\right)^{\frac{2}{3}}}\right]\frac{p_s}{p_{o_2}} + \left[\frac{1}{1+\left(\frac{x-x_s}{D}\right)^{-\frac{2}{3}}}\right]^{\left(\frac{p_s}{p_1}\right)}\cdot\frac{p_1}{p_{o_2}} \quad (2.1)$$

The symbols used in Eq. (2.1) are identified in Fig. 1.

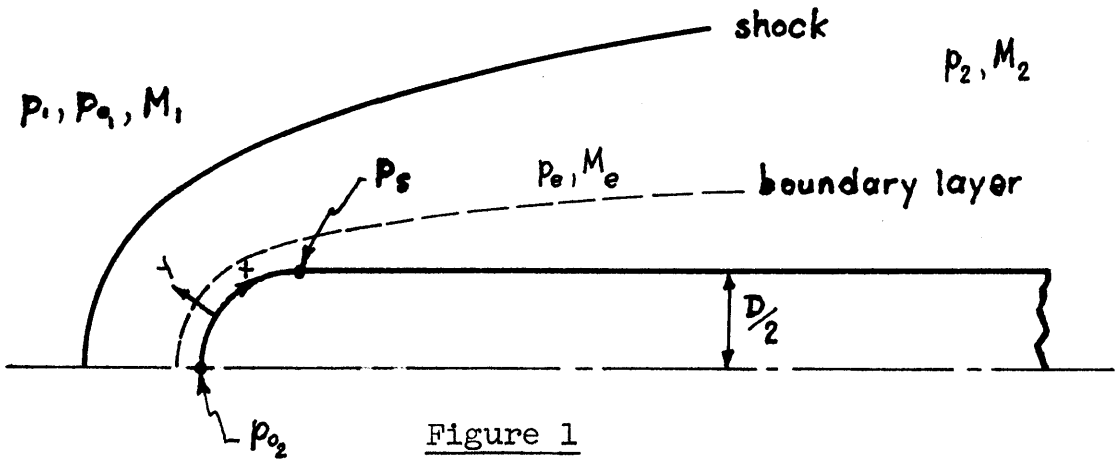

Figure 1

p_s: shoulder static pressure
p_1: free stream static pressure
p_{o_2}: leading edge stagnation pressure
p_2: static pressure far downstream

It should be noted that according to Eq. (2.1),

$$\lim_{\left(\frac{x-x_3}{D}\right)\to\infty} \left(p_e/p_{o_2}\right) = \frac{p_2}{p_{o_2}} = \frac{p_1}{p_{o_2}}$$

This limit is consistent with the fact that as x increases the shock approaches a Mach line, in which case the static pressure approaches the free stream static pressure.

The edge static pressure ratio $\left(p_e/p_{o_2}\right)$ is plotted in Figure 2, using a dimensionless coordinate $\xi = x/D$. Since for these preliminary computations the flow is assumed to be isentropic, all conditions at the edge of the boundary layer may be obtained from the static pressure distribution by using isentropic relationships. For further calculations, the edge Mach number distribution will be particularly useful, and it appears plotted in Figures 3 and 4. Figure 3 shows that up to the shoulder the edge Mach number increases linearly with ξ.

2.3 Momentum Thickness Distribution

In Ref. 6, Rott and Crabtree combine Thwaites' approximate solution to incompressible boundary layers with the Illingworth-Stewartson transformation (Ref. 7), to obtain an explicit formula for the compressible momentum thickness in terms of the conditions at the edge of the boundary layer. Their derivation involves the previously stated assumptions of Prandtl number equal to unity and zero heat transfer at

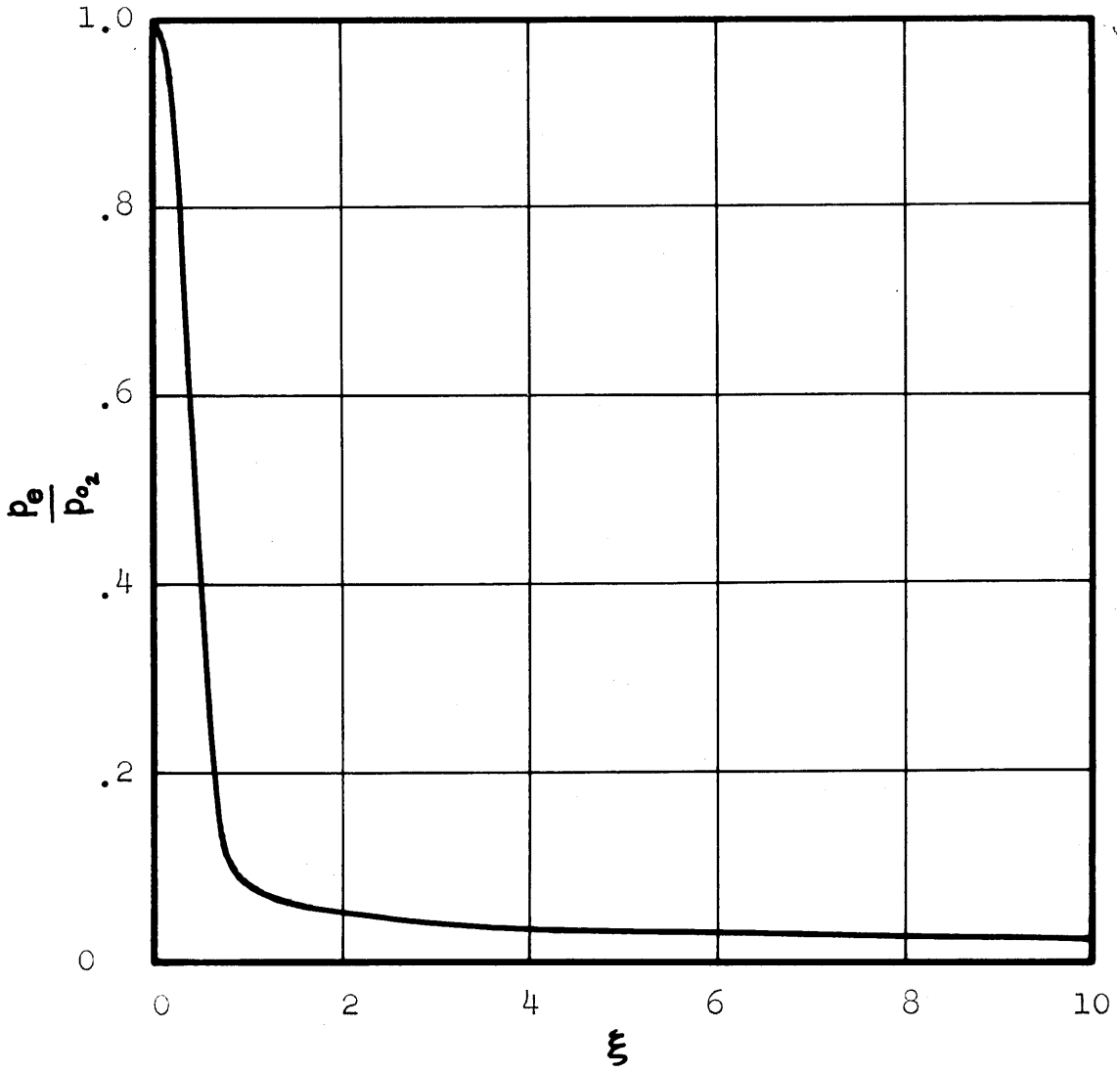

Figure 2 Static Pressure Distribution.

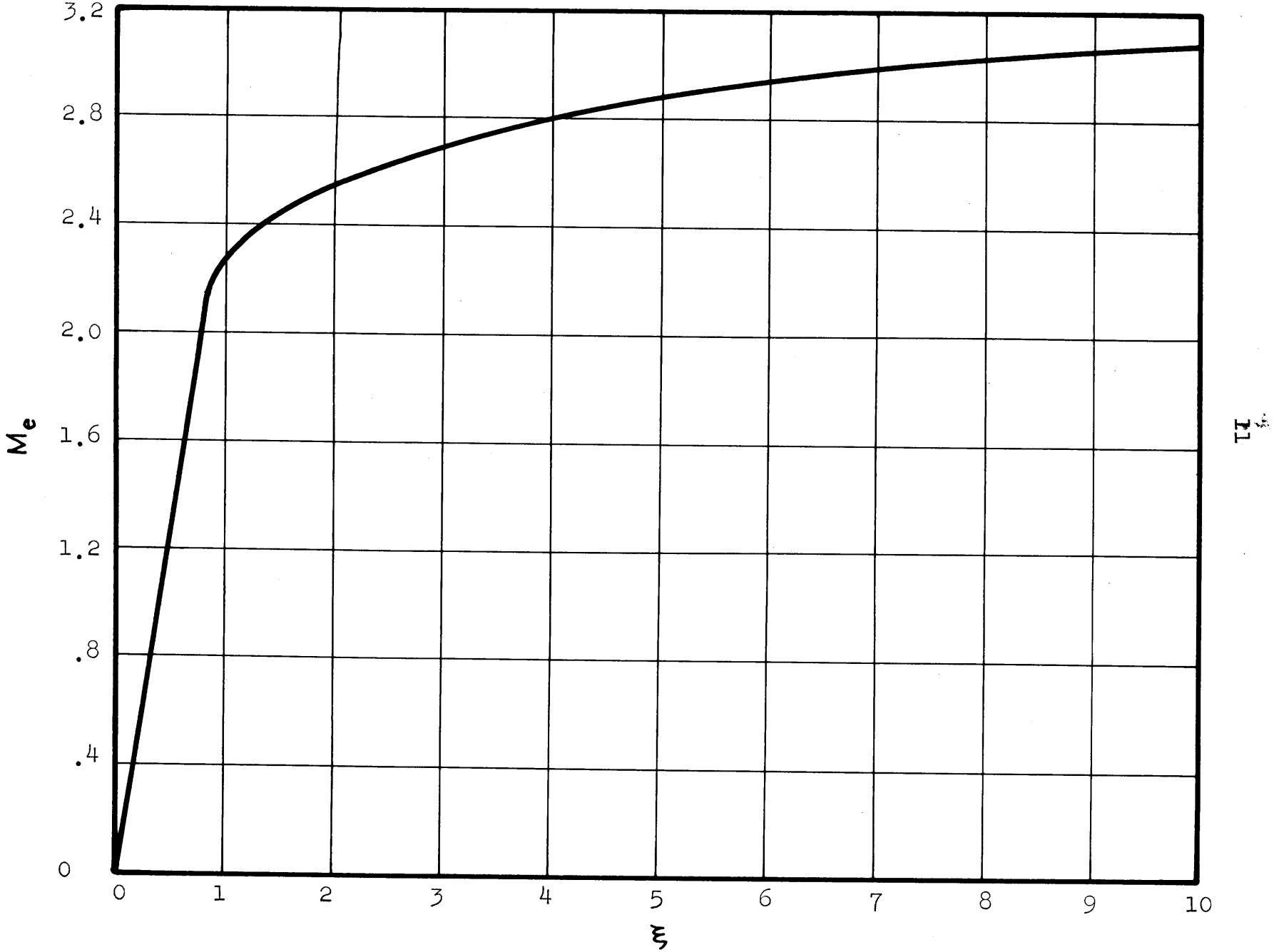

Figure 3 Isentropic Mach Number Distribution.

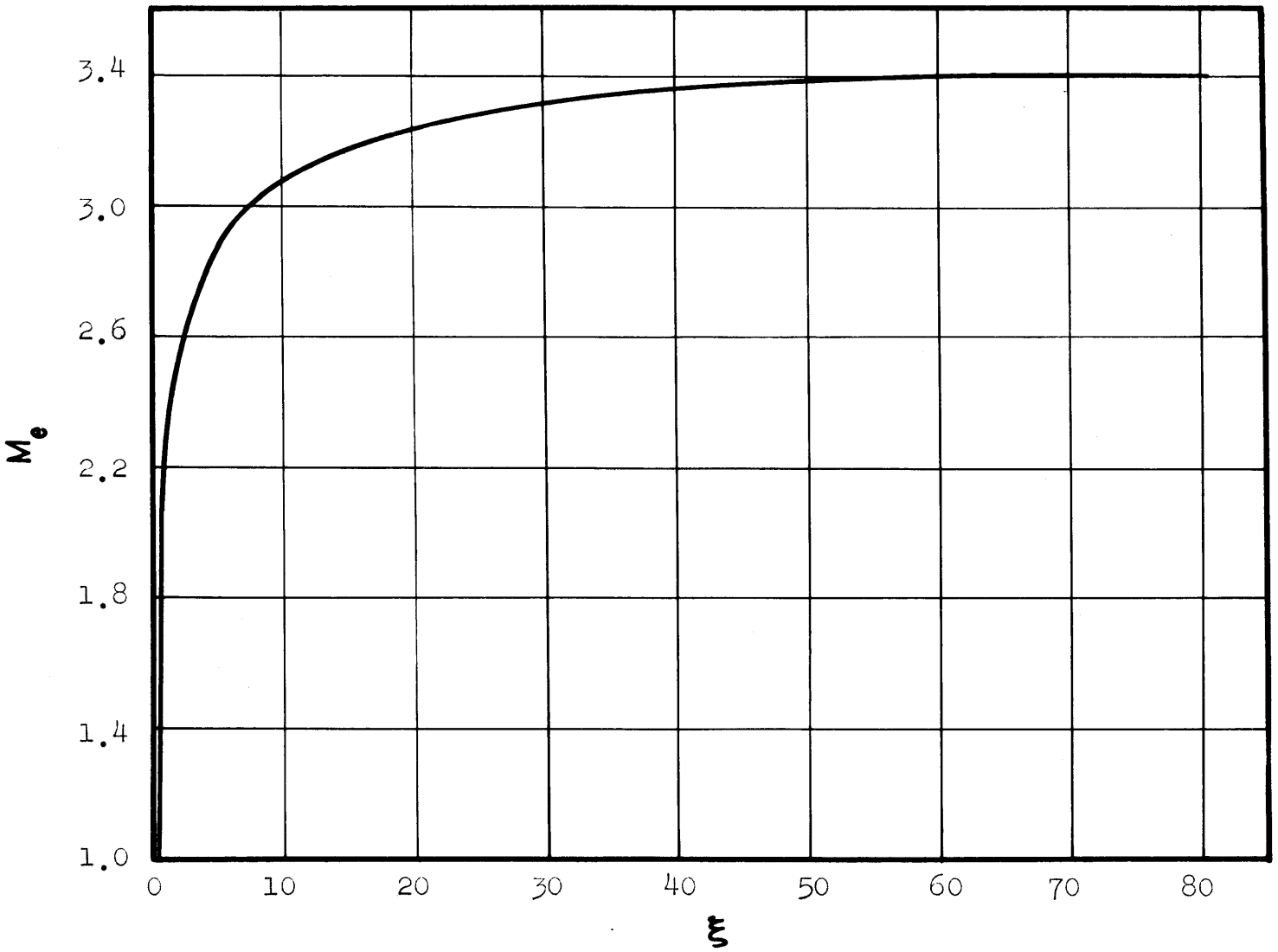

Figure 4 Mach Number Distribution.

the surface, plus the assumption of a linear viscosity-temperature relationship. The expression for the momentum thickness θ given by Rott and Crabtree may be non-dimensionalized to yield:

$$Re_{D_2}\left(\frac{\theta}{D}\right)^2 = .45\left(\frac{T_{o_2}}{T_e}\right)^6 \frac{1}{M_e^6}\int_0^{\xi}\left(\frac{T_e}{T_{o_2}}\right)^4 M_e^5\, d\xi \qquad (2.2)$$

where Re_{D_2} is a stagnation Reynolds number based on conditions at the stagnation point.

$$Re_{D_2} = \frac{a_{o_2}\rho_{o_2}D}{\mu_{o_2}}$$

For purposes of comparison, it will be desirable to express results in terms of the free stream stagnation Reynolds number

$$Re_{D_1} = \frac{a_{o_1}\rho_{o_1}D}{\mu_{o_1}}$$

The relationship between both stagnation Reynolds numbers, using the fact that

$$T_{o_1} = T_{o_2} \quad ; \quad \mu_{o_1} = \mu_{o_2}$$

may be found to be

$$\frac{p_{o_2}}{p_{o_1}} Re_{D_1} = Re_{D_2} \qquad (2.3)$$

and therefore

$$\frac{\theta}{D}\sqrt{Re_{D_1}} = .672\left(\frac{p_{o_1}}{p_{o_2}}\right)^{1/2}\left(\frac{T_{o_2}}{T_e}\right)^{3}\frac{1}{M_e^3}\sqrt{\int_0^{\xi}\left(\frac{T_e}{T_{o_2}}\right)^{4}M_e^5\,d\xi} \qquad (2.3)$$

Equation (2.3) becomes indeterminate at $\xi = 0$, and the stagnation point was therefore treated as follows: From Fig. 3 it is evident that near the stagnation point M_e is directly proportional to ξ . Therefore, if

$$M_e = \beta\xi \quad ; \qquad \beta = \text{constant}$$

and ξ is small so that $M_e^2 \ll 1$, and consequently $\frac{T_e}{T_{o_2}} \approx 1$.; equation (2.3) becomes

$$\frac{\theta}{D}\sqrt{Re_{D_1}} = .672\left(\frac{p_{o_1}}{p_{o_2}}\right)^{1/2}\frac{1}{\beta^3\xi^3}\sqrt{\int_0^{\xi}\beta^5\xi^5\,d\xi}$$

or

$$\left[\frac{\theta}{D}\sqrt{Re_{D_1}}\right]_{\xi=0} = \sqrt{\frac{.45}{6\beta}}\left(\frac{p_{o_1}}{p_{o_2}}\right)^{1/2}$$

β may be found to have a value of 2.46 from Fig. 3 and therefore

$$\left[\frac{\theta}{D}\sqrt{Re_{D_1}}\right]_{\xi=0} = 1.70 \qquad (2.4)$$

Equations (2.3) and (2.4) are plotted in Figures 5 and 6 .

For the sharp and constant-pressure isentropic blunt plates, the boundary layer edge conditions do not depend on ξ , and Eq. (2.3) may then be integrated to yield

$$\left[\frac{\theta}{D}\sqrt{Re_{D_1}}\right]_{S.P.} = \frac{.672}{\sqrt{M_1}}\left(\frac{T_{o_1}}{T_1}\right)\sqrt{\xi} \qquad (2.5)$$

for the sharp plate, and

$$\left[\frac{\theta}{D}\sqrt{Re_{D_1}}\right]_{C.P.-C.E.} = \frac{.672}{\sqrt{M_2}}\sqrt{\frac{p_{o_1}}{p_{o_2}}}\left(\frac{T_{o_2}}{T_2}\right)\sqrt{\xi} \qquad (2.6)$$

for the constant-pressure blunt plate. These parabolic expressions for θ/D also appear plotted in Figures 5 and 6 .

2.4 Displacement Thickness Distribution

Following Thwaites' method, the boundary layer displacement thickness may be obtained from its momentum thickness by calculating the parameter m , which is related to the second derivative of the velocity distribution at the surface. The calculation of m will then yield another parameter H , which is the ratio of displacement to momentum thickness. Since Thwaites' results hold for <u>incompressible</u> boundary layers, it is necessary

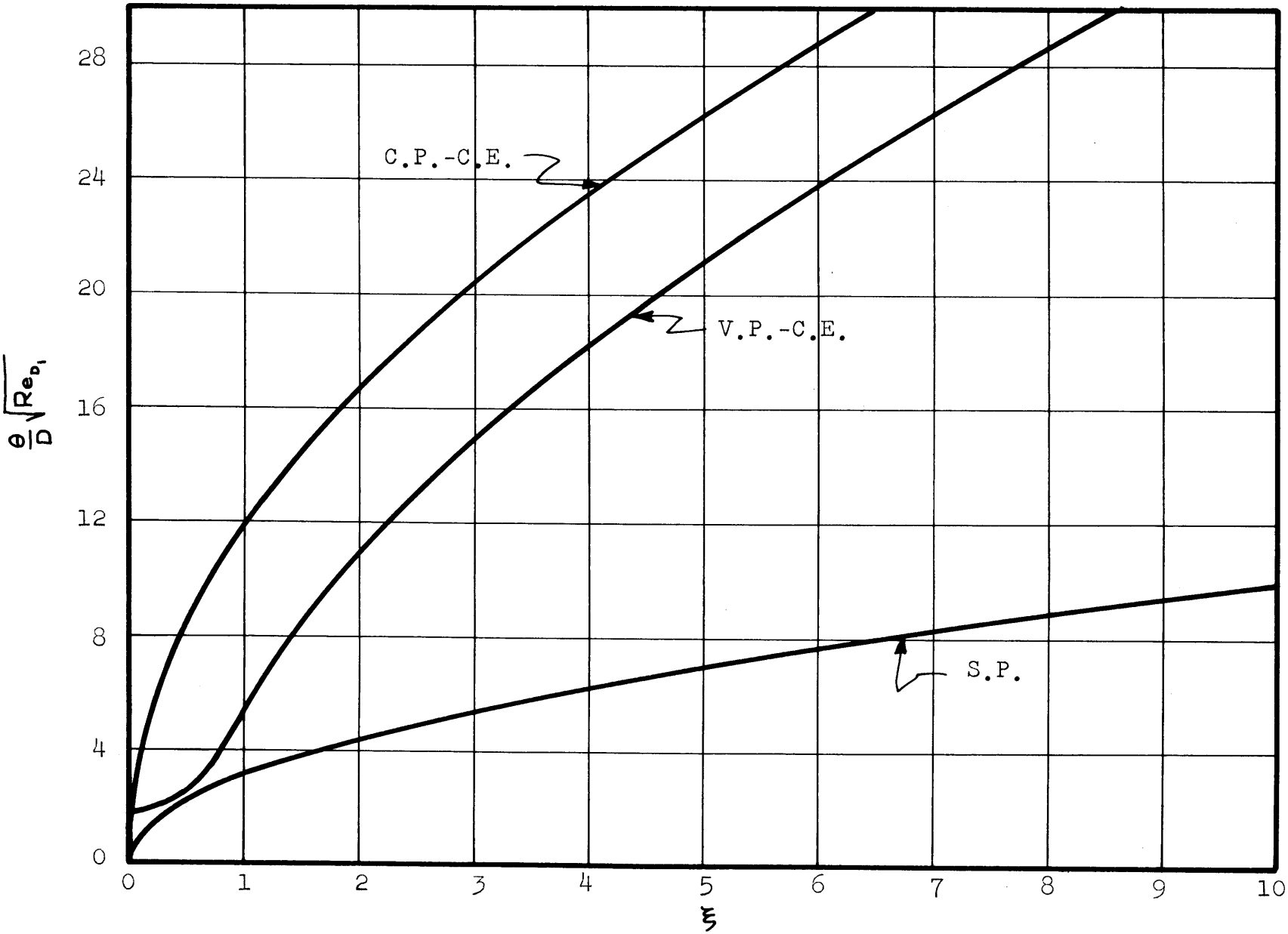

Figure 5 Momentum Thickness Distribution.

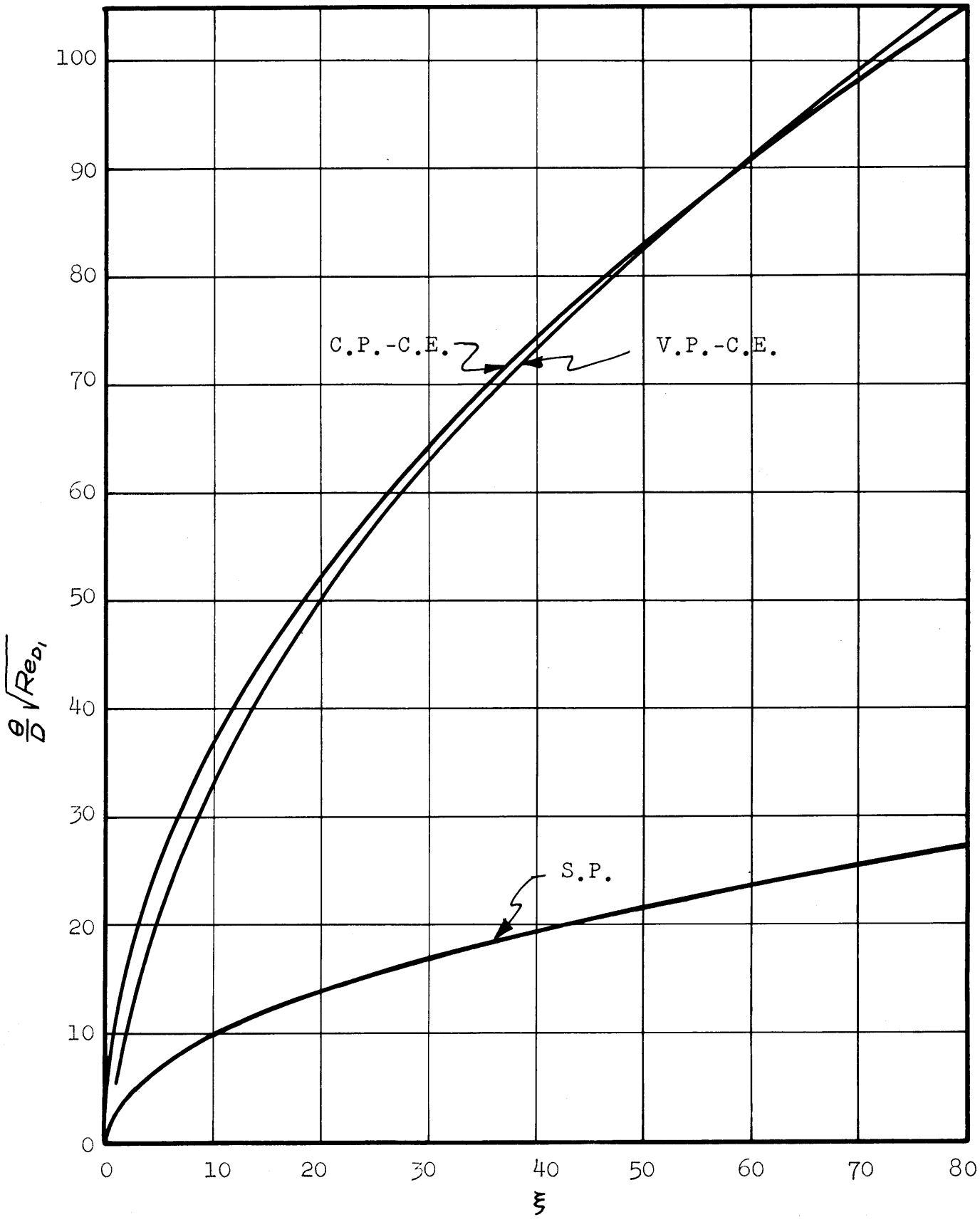

Figure 6 Momentum Thickness Distribution.

to reduce the compressible parameter m to an incompressible m_s ; with this m_s calculate the incompressible H_s ; and finally transform this H_s back to a compressible

$$H = \frac{\delta^*}{\theta}$$

The relationships between compressible and incompressible parameters are again given by Rott and Crabtree in Ref. 7. For m_s this is

$$m_s = -\frac{dU_e}{dx}\frac{\rho_{o_2}}{\mu_{o_2}}\theta^2\left(\frac{T_e}{T_{o_2}}\right)^{1/2}$$

Using the fact that

$$\frac{dU_e}{dx} = a_e\frac{dM_e}{dx} + M_e\frac{da_e}{dx}$$

the expression for m_s may be written in terms of the edge Mach number, the temperature ratio, a non-dimensional momentum thickness, and a grouping of terms which - not surprisingly - turns out to be the stagnation Reynolds number Re_{o_2} . Then writing Re_{D_2} in terms of Re_{D_1} ; m_s becomes

$$m_s = -\left[\frac{\theta}{D}\sqrt{Re_{D_1}}\right]\left(\frac{p_{o_1}}{p_{o_2}}\right)\left(\frac{T_e}{T_{o_2}}\right)^2\frac{dM_e}{d\xi} \qquad (2.7)$$

Table I in Thwaites' paper (Ref. 5) will then yield the incompressible parameter H_s . The compressible H may finally be obtained from a relationship given by Rott and Crabtree.

$$\frac{\delta^*}{\theta} = H = H_s\left(\frac{T_{o_2}}{T_e}\right) + \frac{T_{o_2}}{T_e} - 1 \qquad (2.8)$$

Finally, the non-dimensional displacement thickness is obtained from

$$\frac{\delta^*}{D}\sqrt{Re_{D_1}} = H\,\frac{\theta}{D}\sqrt{Re_{D_1}}$$

For the sharp and the constant-pressure blunt plates m_s will be zero because $dM_e/d\xi = 0$. Thwaites' Table I then gives a value for H_s of 2.61.

The compressible H's will be given by

$$H_{s.p.} = H_s\left(\frac{T_{o_2}}{T_1}\right) + \frac{T_{o_2}}{T_1} - 1 \qquad (2.9a)$$

and

$$H_{c.p.-c.t.} = H_s\left(\frac{T_{o_2}}{T_2}\right) + \frac{T_{o_2}}{T_2} - 1 \qquad (2.9b)$$

The displacement thickness distribution may then be obtained for these two cases by merely multiplying the momentum thickness distributions by the constant factors given by Eqs. (2.9a) and (2.9b).

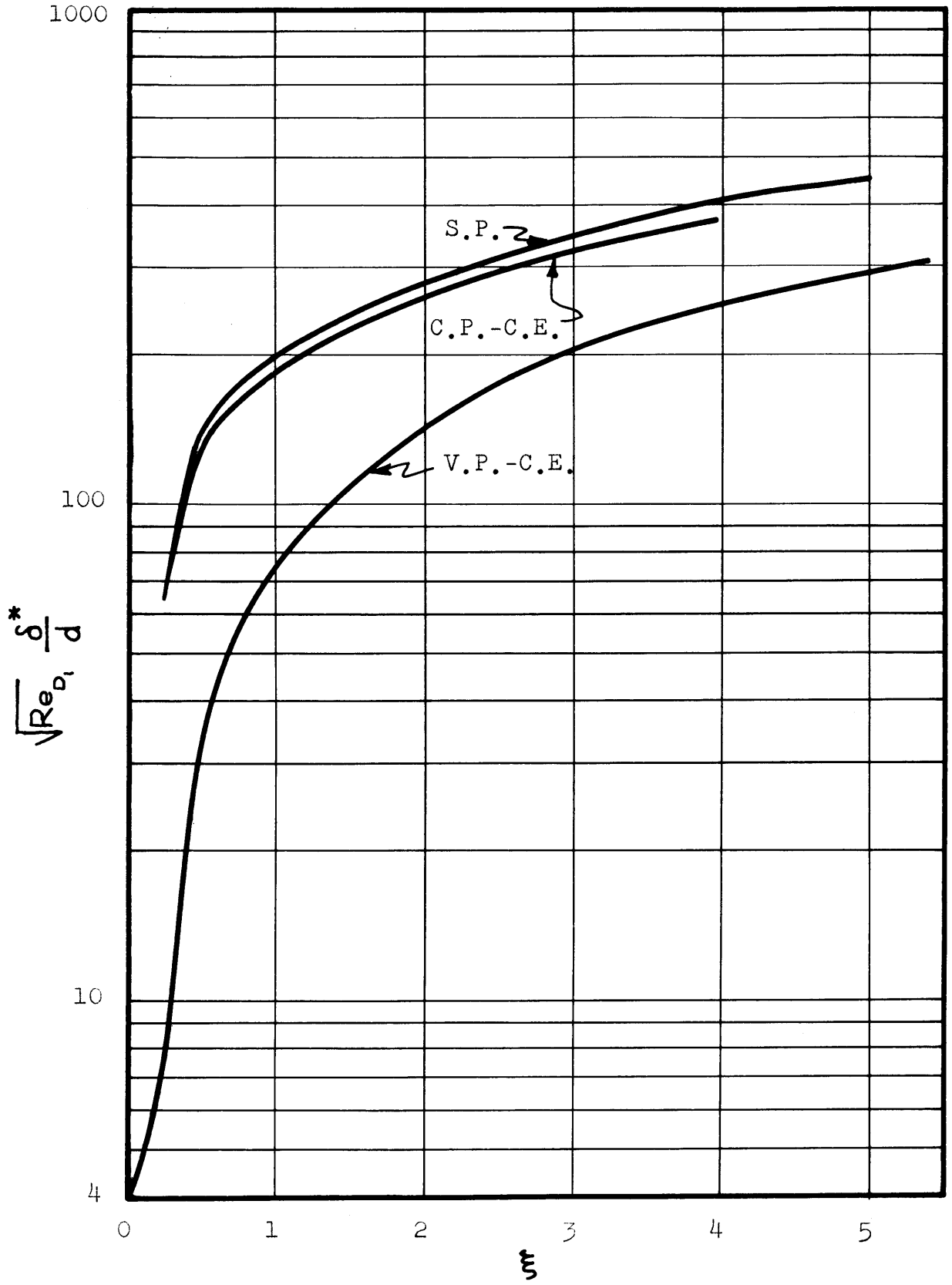

Figure 7 Displacement Thickness Distribution.

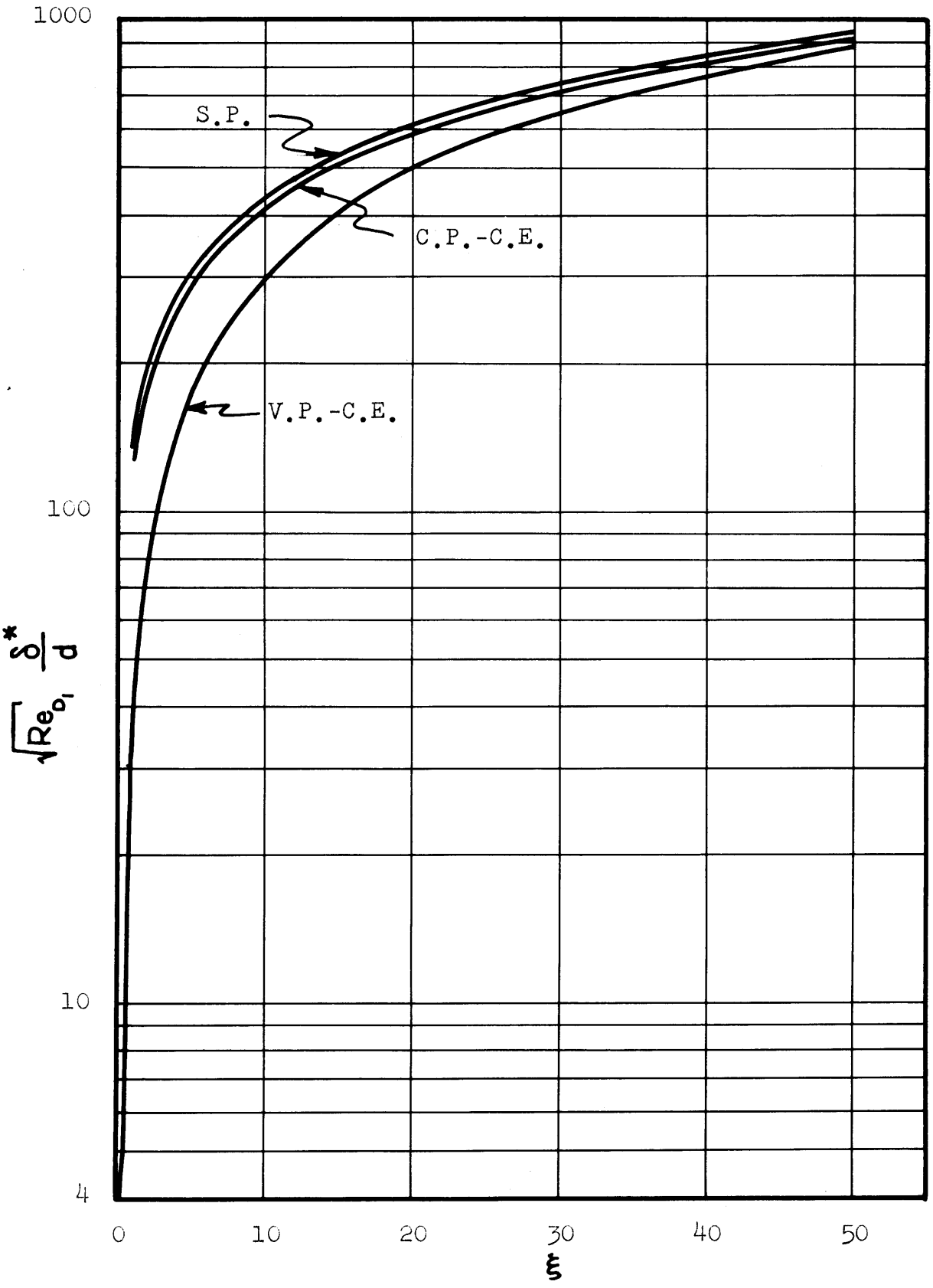

Figure 8 Displacement Thickness Distribution.

The non-dimensionalized displacement thicknesses for all three cases appear in Figures 7 and 8 .

2.5 Boundary Layer Pressure Influence

As suggested in the introduction, the pressure correction due to the boundary layer is estimated by considering an inviscid body whose thickness has been increased by the displacement thickness, and estimating the pressure increment produced by a Prandtl-Meyer expansion about this new inviscid body. Figure 9 illustrates this approach.

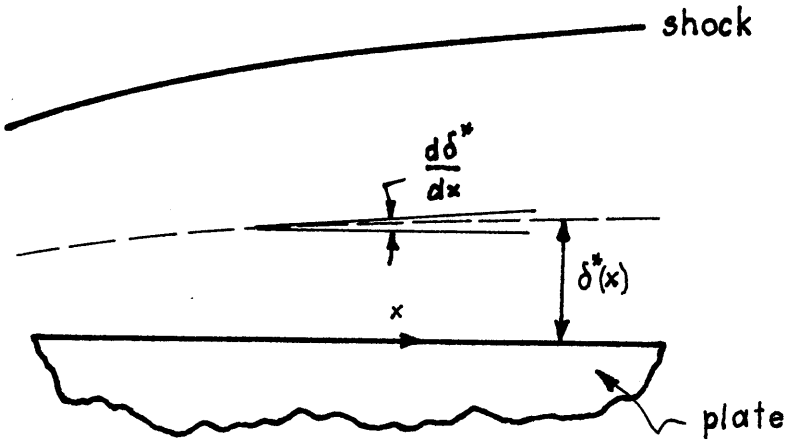

Figure 9

The local inviscid body inclination is assumed to be equal to the slope of the displacement thickness at the point of interest, and it is therefore necessary to obtain the displacement thickness slope distribution along the plate.

Since

$$\frac{\delta^*}{D}\sqrt{Re_{D_1}} = H\frac{\theta}{D}\sqrt{Re_{D_1}}$$

it follows that

$$\sqrt{Re_{D_1}}\,\frac{d(\delta^*/D)}{d\xi} = \frac{\theta}{D}\sqrt{Re_{D_1}}\,\frac{dH}{d\xi} + H\sqrt{Re_{D_1}}\,\frac{d(\theta/D)}{d\xi} \qquad (2.10)$$

From Eq. (2.3)

$$\sqrt{Re_{D_1}}\,\frac{d(\theta/D)}{d\xi} = .672\left(\frac{p_{o_1}}{p_{o_2}}\right)^{1/2}\left\{\frac{1}{2}\left(\frac{T_{o_2}}{T_e}\right)^3\frac{\left(\frac{T_e}{T_{o_2}}\right)^4 M_e^2}{\sqrt{\int_0^\xi\left(\frac{T_e}{T_{o_2}}\right)^4 M_e^5\,d\xi}} + \right.$$

$$\left. + \sqrt{\int_0^\xi\left(\frac{T_e}{T_{o_2}}\right)^4 M_e^5\,d\xi}\;\;\frac{d}{d\xi}\left[\left(\frac{T_{o_2}}{T_e}\right)^3\frac{1}{M_e^3}\right]\right\} \qquad (2.11)$$

Expanding the derivative in the last term and collecting terms, (2.11) may be written as

$$\sqrt{Re_{D_1}}\,\frac{d(\theta/D)}{d\xi} = \frac{.672\left(p_{o_1}/p_{o_2}\right)^{1/2}}{\sqrt{\int_0^\xi\left(\frac{T_e}{T_{o_2}}\right)^4 M_e^5\,d\xi}}\left\{\frac{T_e}{T_{o_2}}\,\frac{M_e^2}{2} + \right.$$

$$\left. + \left[\int_0^\xi\left(\frac{T_e}{T_{o_2}}\right)^4 M_e^5\,d\xi\right]\cdot\frac{3}{M_e^4}\left(\frac{T_{o_2}}{T_e}\right)^2\frac{dM_e}{d\xi}\left[\frac{T_{o_2}}{T_e} - 2\right]\right\}$$

and substituting for $\frac{d(\theta/D)}{d\xi}\sqrt{Re_{D_1}}$ in (2.10), the final expression becomes

$$\frac{d(\delta^*/D)}{d\xi}\sqrt{Re_{D_1}} = \frac{\theta}{D}\sqrt{Re_{D_1}}\frac{dH}{d\xi} + \frac{.672\,H}{\sqrt{\int_0^\xi \left(\frac{T_e}{T_{o_2}}\right)^4 M_e^5\, d\xi}}\left(\frac{p_{o_1}}{p_{o_2}}\right)^{1/2} \cdot \tag{2.12}$$

$$\cdot\left\{\frac{T_e}{T_{o_2}}\frac{M_e^2}{2} + \frac{3}{M_e^4}\left(\frac{T_{o_2}}{T_e}\right)^2\frac{dM_e}{d\xi}\left[\int_0^\xi \left(\frac{T_e}{T_{o_2}}\right)^4 M_e^5\, d\xi\right]\left[\frac{T_{o_2}}{T_e} - 2\right]\right\}$$

For the sharp and isentropic constant-pressure blunt plates, H and M_e are constants and the terms involving their derivatives in Eq. (2.12) will drop out. The expression then reduces to

$$\left[\frac{d(\delta^*/D)}{d\xi}\sqrt{Re_{D_1}}\right]_{S.P.} = \frac{.336}{\sqrt{M_1}}\,H_1\left(\frac{T_{o_1}}{T_1}\right)\frac{1}{\sqrt{\xi}} \tag{2.13}$$

for the sharp plate and

$$\left[\frac{d(\delta^*/D)}{d\xi}\sqrt{Re_{D_1}}\right]_{C.P.\text{-}C.E.} = \frac{.336}{\sqrt{M_2}}\,H_2\left(\frac{p_{o_1}}{p_{o_2}}\right)^{1/2}\left(\frac{T_{o_2}}{T_2}\right)\frac{1}{\sqrt{\xi}} \tag{2.14}$$

for the constant-pressure blunt plate.

Using the Prandtl-Meyer expansion approximation to calculate the pressure influence of the boundary layer, the non-dimensional pressure influence $\Delta p/p_e$ is given to the first order by

$$\frac{\Delta p}{p_e}\sqrt{Re_{D_1}} \cong \frac{\gamma M_e^2}{(M_e^2-1)^{1/2}}\sqrt{Re_{D_1}}\,\frac{d(\delta^*/D)}{d\xi_1} \qquad (2.15)$$

To provide a common reference for purposes of comparison, it is desirable to evaluate the ratio $\Delta p/p_{o_2}$ which is given by

$$\frac{\Delta p}{p_{o_2}}\sqrt{Re_{D_1}} = \frac{p_e}{p_{o_2}}\left[\frac{\Delta p}{p_e}\sqrt{Re_{D_1}}\right] \qquad (2.16)$$

For the sharp plate, Eq. (2.16) becomes

$$\left[\frac{\Delta p}{p_{o_2}}\sqrt{Re_{D_1}}\right]_{S.P.} = \frac{\gamma M_1^2}{(M_1^2-1)^{1/2}}\,\frac{p_e}{p_{o_2}}\,\frac{p_{o_1}}{p_{o_2}}\left[\sqrt{Re_{D_1}}\,\frac{d(\delta^*/D)}{d\xi_1}\right]_{S.P.} \qquad (2.17)$$

and for the constant-pressure blunt plate

$$\left[\frac{\Delta p}{p_{o_2}}\sqrt{Re_{D_1}}\right]_{C.P.-C.E.} = \frac{\gamma M_2^2}{(M_2^2-1)^{1/2}}\,\frac{p_2}{p_{o_2}}\left[\sqrt{Re_{D_1}}\,\frac{d(\delta^*/D)}{d\xi_1}\right]_{C.P.-C.E.} \qquad (2.18)$$

Equations (2.16), (2.17) and (2.18) may now be evaluated by using the corresponding expressions for $\left[\sqrt{Re_{D_1}}\,\frac{d(\delta^*/D)}{d\xi_1}\right]$ They are plotted in Figures 10 and 11 .

In order to evaluate the boundary layer pressure influence at the particular testing conditions for which experiments were carried out at the Aerophysics Laboratory,

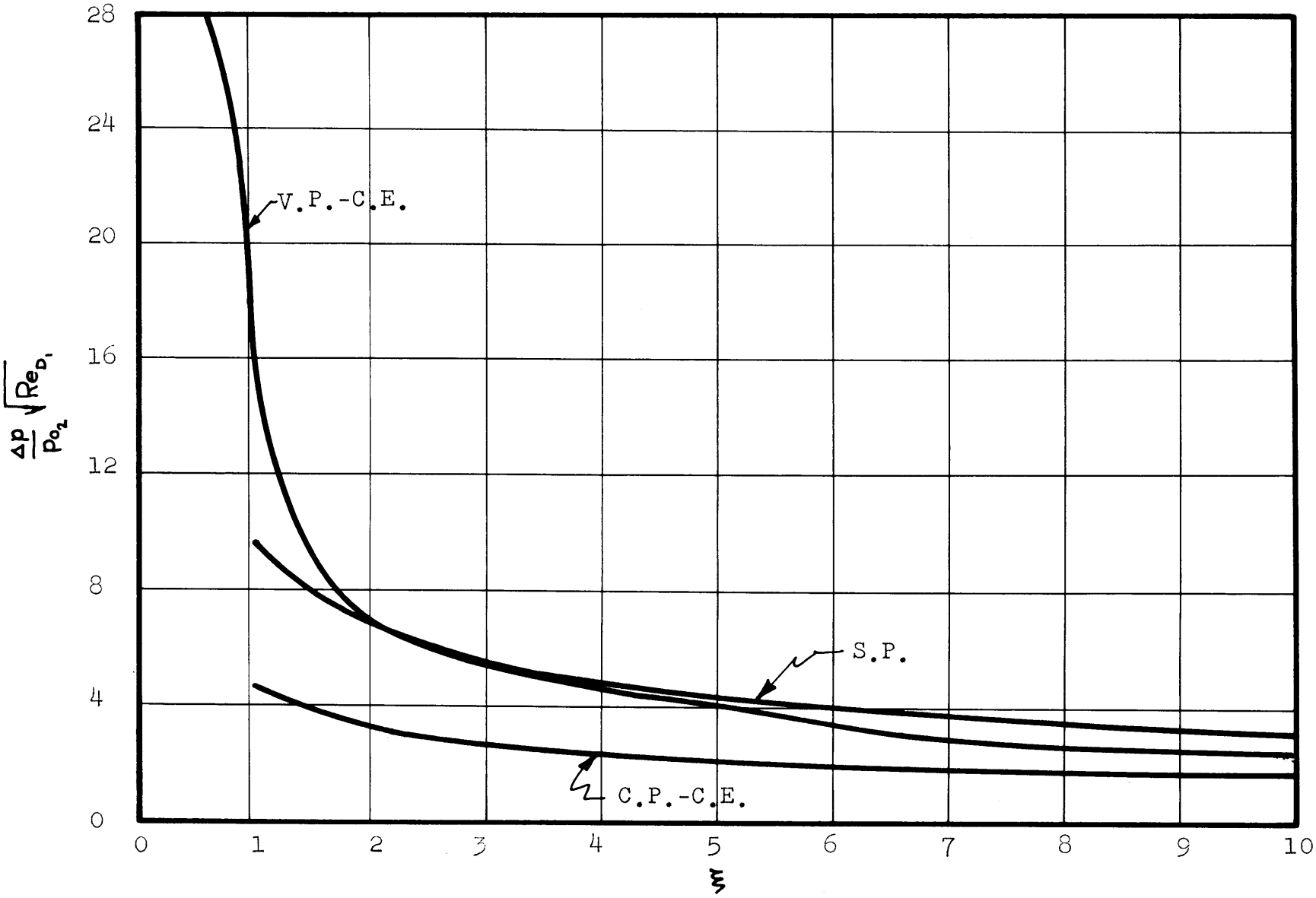

Figure 10 Pressure Increment Distribution.

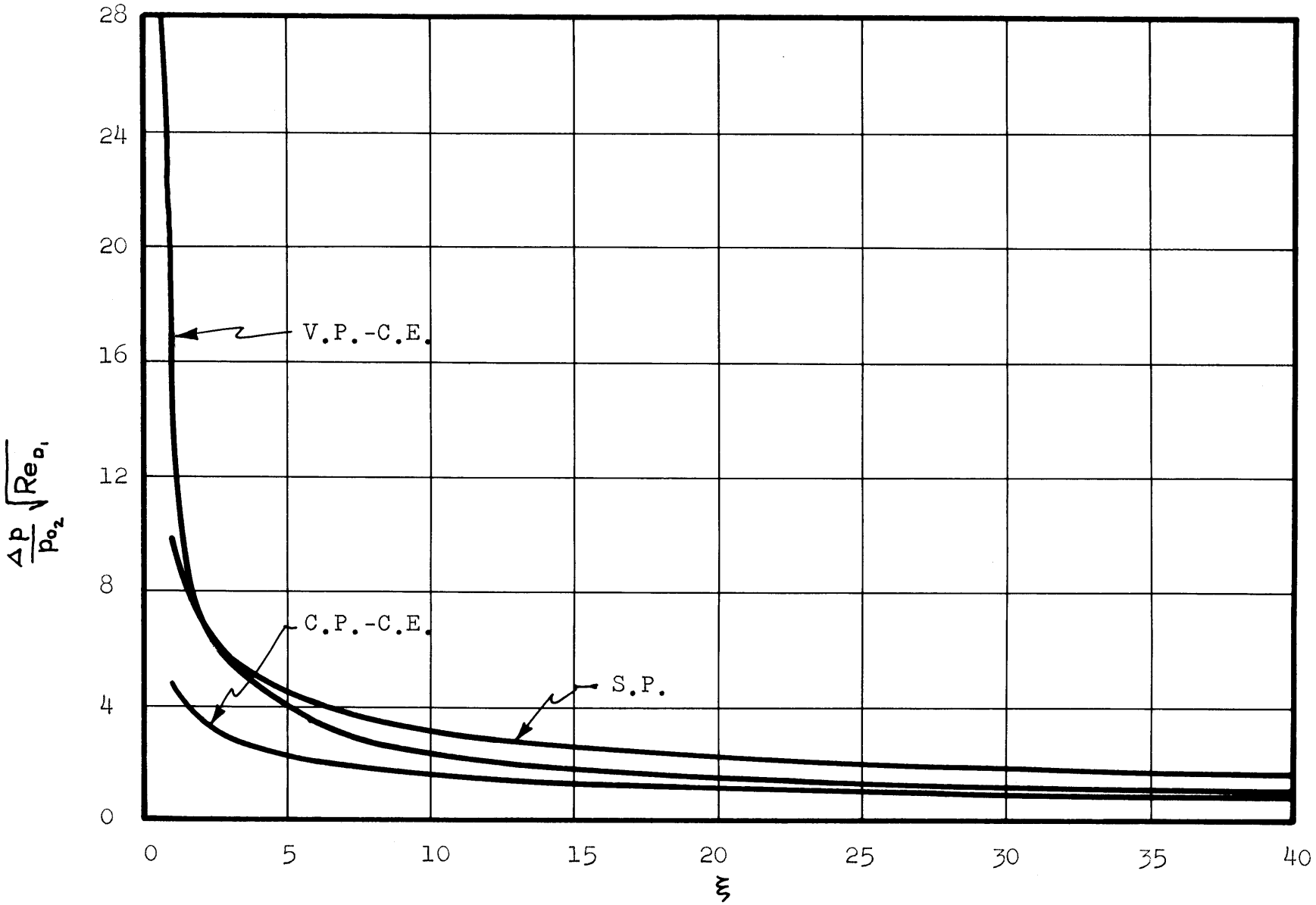

Figure 11 Pressure Increment Distribution.

it is necessary to calculate the free stream stagnation Reynolds number Re_{D_1} . The test conditions were

$$M_1 = 7.6 \qquad T_{0_1} = 1210\ ^\circ F\ abs.$$

$$p_{0_1} = 100\ psia. \qquad D = 3/8\ in.$$

With these quantities, the free stream stagnation Reynolds number is found to have a value of

$$Re_{D_1} = 95,700$$

With this value of the Reynolds number the pressure disturbance for the blunt plate is plotted in Fig. 12 . It may be seen to be everywhere smaller than 10%; and to become very small for values of ξ greater than 7 or 8.

2.6 Discussion of Isentropic Results

Figures 5 and 6 show that the momentum thickness distribution for the blunt plate may be closely approximated at the higher values of ξ by that for the constant-pressure blunt plate. The momentum thickness for the sharp plate is seen to be considerably smaller than for the other two plates, over the entire range of ξ . Figure 8 shows, however, that at the higher values of ξ , all three displacement thickness distributions lie very close together, including the sharp plate displacement thickness. This may be explained

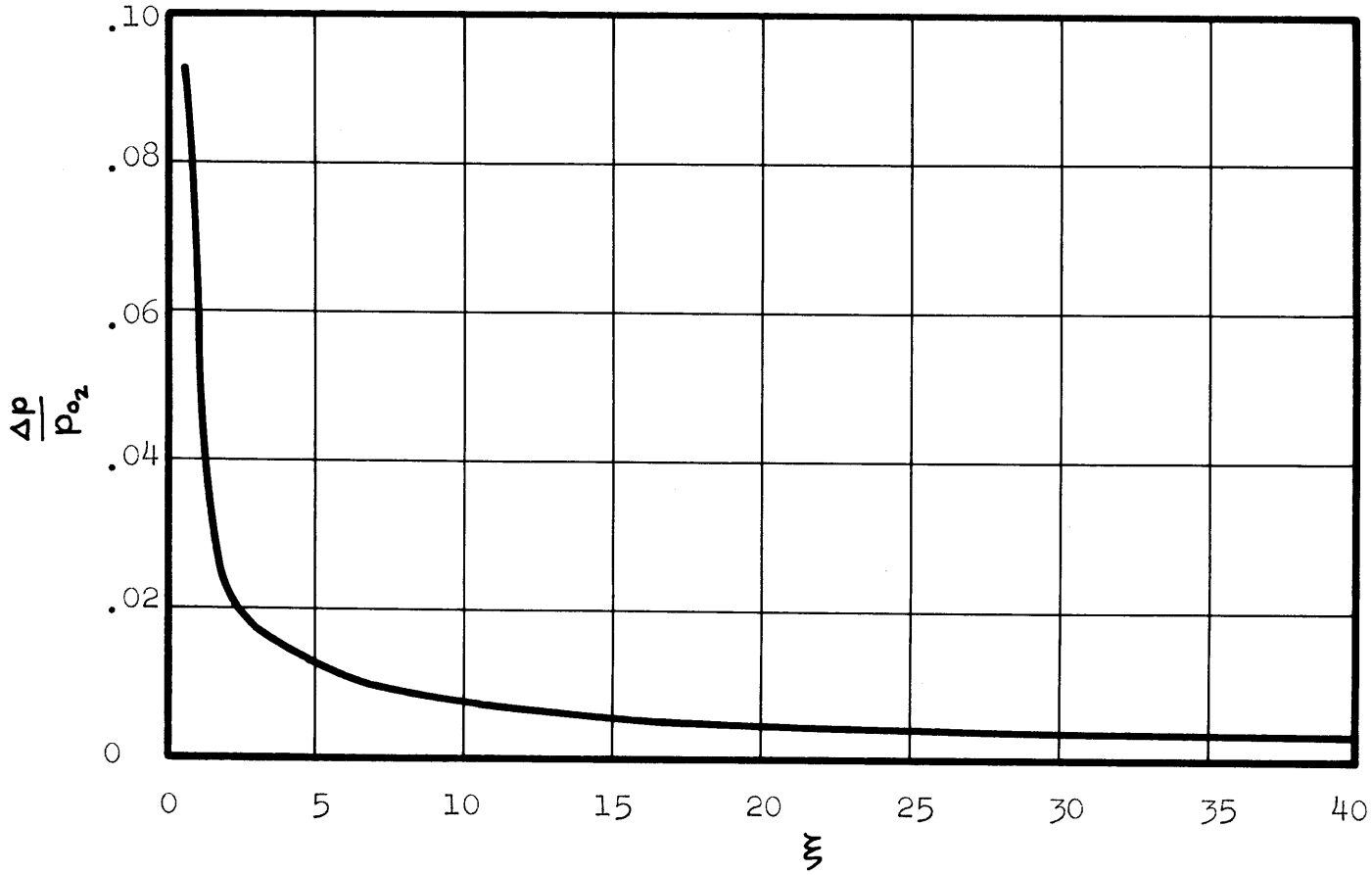

Figure 12 Boundary Layer Pressure Disturbance for $M_1 = 7.6$, $Re_{D_1} = 95,700$ on the Isentropic Blunt Plate.

by examining the transformation of the compressible H for the sharp plate. This was

$$H = H_s \frac{T_{o_1}}{T_1} + \frac{T_{o_1}}{T_1} - 1$$

Since T_{o_1}/T_1 is greater than T_{o_2}/T_e or T_{o_2}/T_2, H will be greater for the sharp plate than for the other two cases; this will tend to cancel out the effect of a smaller θ/D and make the displacement thickness for the sharp plate roughly equivalent to that for the other two cases.

The calculations performed for the isentropic case have shown that it is possible to approximate the actual blunt plate by a fictitious blunt plate with a constant surface static pressure equal to the free stream static pressure. Since the results show that this approximation becomes particularly good at large values of ξ_1 - which is precisely the region where non-isentropic effects become important - the calculations suggest that it may be possible to replace the actual non-isentropic plate by a fictitious constant-pressure non-isentropic plate, and thus considerably simplify the solution of the non-isentropic case. Because the solution is simpler, the variable entropy case will be first solved under the assumption that the static pressure remains constant along the plate, at a value equal to the

free stream value. The complete variable-pressure, variable-entropy case will be solved last, and these more exact results will be compared to the simpler, constant pressure approximations.

The calculations for the isentropic sharp plate have provided an upper asymptote which the non-isentropic results should approach as the coordinate ξ approaches infinity.

CHAPTER 3

DERIVATION OF PERTINENT BOUNDARY LAYER EQUATIONS

3.1 As discussed in Chapter 2, the boundary layer along a blunt plate submerged in a hypersonic stream will have non-isentropic edge conditions. The static pressure will be assumed to vary as in the isentropic case, but the curved bow shock will produce a variation of stagnation pressure which does not occur in the isentropic case. The non-isentropic edge conditions should approach isentropic values near the leading edge and far downstream from the leading edge.

The solution of the variable entropy problem differs from the solution of the isentropic case in two respects. First, the velocity at the edge of the boundary layer cannot be obtained directly from the static pressure distribution, because Bernoulli's equation does not apply. Secondly, Bernoulli's equation cannot be used in the solution or transformation of the boundary layer momentum equation.

Figure 13 illustrates the pertinent variables and reference quantities for the variable entropy problem. Along the streamline a , the entropy is constant and stagnation conditions are therefore constant. If a shock

$( )_1$: Free stream conditions

$( )_{O_2}$: Leading edge stagnation point conditions

$( )_e$: Boundary layer edge conditions

$( )_{O_e}$: Boundary layer stagnation edge conditions

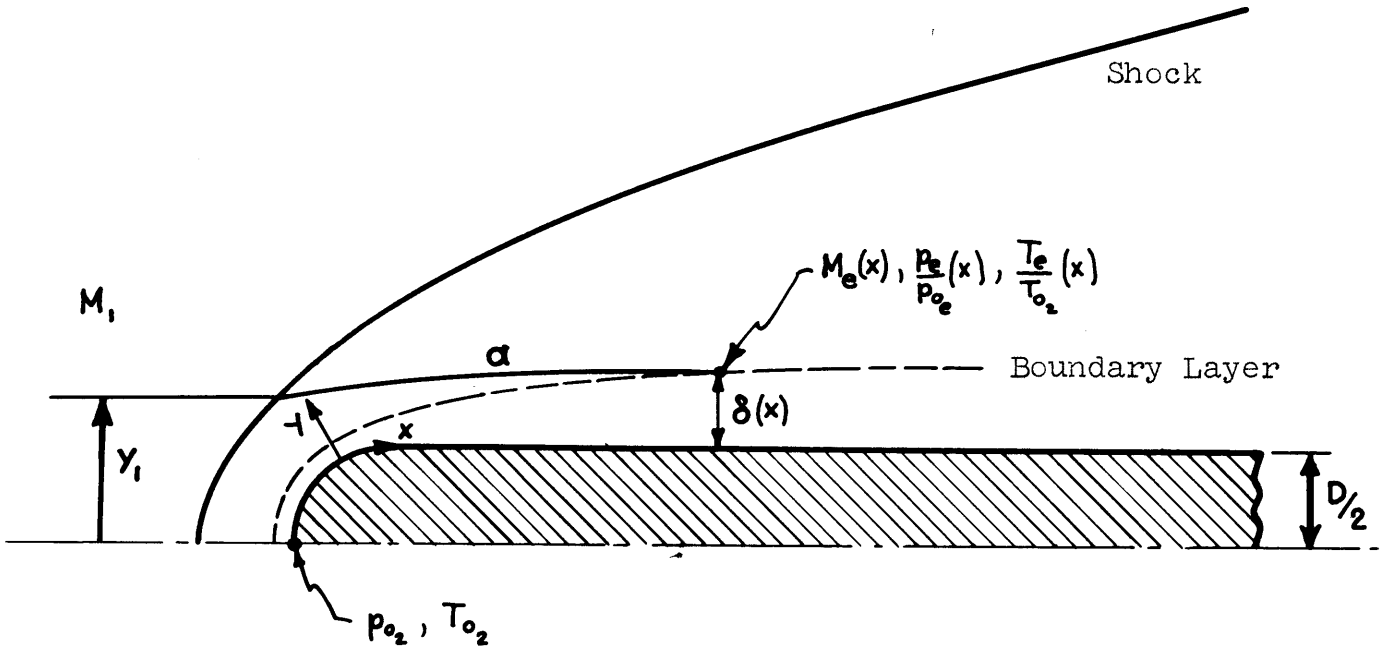

Figure 13 Variables and Reference Quantities for the Variable Entropy Problem.

shape is assumed it is possible to obtain the stagnation conditions immediately behind the shock (at y_1) because the local shock inclination angle will be known. These stagnation conditions will correspond to the edge stagnation conditions at the point where the streamline a intersects the boundary layer. This discussion suggests that it is therefore possible to obtain the variation of boundary layer edge conditions with x by relating the streamline-shock intersection height y_1 to the spatial variable x.

3.2 Energy Equation

The assumptions of Prandtl number equal to unity and zero heat transfer at the wall lead to a simple expression for the temperature distribution in the boundary layer.

$$\frac{T}{T_e} = 1 + \frac{\gamma-1}{2} M_e^2 \left(1 - \frac{u^2}{U_e^2}\right) \qquad (3.1)$$

Since at the surface of the plate the velocity is zero, the temperature T_w at the surface is simply given by

$$\frac{T_w}{T_e} = 1 + \frac{\gamma-1}{2} M_e^2 = \frac{T_{o_2}}{T_e} = \frac{T_{o_1}}{T_e} \qquad (3.2)$$

3.3 Momentum Integral

The purpose of integral methods is to reduce the boundary layer continuity and momentum partial differential equations to total differential equations, by integration with respect to the y coordinate and the introduction of integral properties of the boundary layer. The boundary layer equations are

Continuity:
$$\frac{\partial(\rho u)}{\partial x} + \frac{\partial(\rho v)}{\partial y} = 0 \tag{3.3}$$

Momentum:
$$\rho\left[u\frac{\partial u}{\partial x} + v\frac{\partial u}{\partial y}\right] = -\frac{dp_e}{dx} + \frac{\partial}{\partial y}\left(\mu\frac{\partial u}{\partial y}\right) \tag{3.4}$$

If the boundary layer thickness δ is defined as the value of y for which the velocity in the boundary layer is very close to the free stream velocity ("very close" meaning a ratio (u/U_e) of approximately .999), Eq. (3.4) may be integrated with respect to y from $y=0$ to $y=\delta$ to give

$$\int_0^\delta \rho u\frac{\partial u}{\partial x}\,dy + \int_0^\delta \rho v\frac{\partial u}{\partial y}\,dy = -\int_0^\delta \frac{dp_e}{dx}\,dy - \mu_w\left(\frac{\partial u}{\partial y}\right)_{y=0} \tag{3.5}$$

It should be noted that the last term on the right-hand side of (3.5) involves the assumption that

$$\left[\mu_e\ \frac{\partial U_e}{\partial y}\right]_{y=\delta} = 0$$

This is not strictly true, because the entropy gradient normal to the surface will produce an inviscid velocity gradient. However, as mentioned in Chapter 1, the Reynolds number considered is high enough to permit the assumption that

$$\left[\frac{\partial U_e}{\partial y}\right]_{y=\delta} \ll \left[\frac{\partial u}{\partial y}\right]_{y=0}$$

and consequent neglect of the inviscid velocity gradient compared to the viscous velocity gradient.

After some algebraic manipulation described in detail in Appendix A, the boundary layer momentum equation may be written as

$$-\frac{d}{dx}\left[\rho_e U_e \theta\right] + \rho_e U_e \frac{dU_e}{dx}(\delta - \delta^*) + \frac{dp_e}{dx}\delta = -\mu_{o_2}\left(\frac{\partial u}{\partial y}\right)_{y=0} \quad (3.6)$$

where θ : momentum thickness

δ^* : displacement thickness

δ : thickness

which is the integrated momentum equation, and which will reduce to the Karman momentum integral for the isentropic case, where

$$\frac{dp_e}{dx} = -\rho_e U_e \, dU_e/dx$$

From (3.4), since at $y = 0$; $u = 0, v = 0$

$$\frac{dp_e}{dx} = \mu_{o_2} \left(\frac{\partial^2 u}{\partial^2 y}\right)_{y=0} \tag{3.7}$$

3.4 Transformation of Momentum Integral

In subsequent work, use will be made of the relationship found by Thwaites[5] between the first and second derivatives of the velocity at the surface, and the ratio of displacement to momentum thickness. Since Thwaites' results hold for incompressible boundary layers, it is necessary to find some relationship between the compressible boundary layer variables and those of an equivalent incompressible boundary layer. This is accomplished, following Hammitt[4], by the use of the Howarth transformation, which replaces the coordinate y by a coordinate S such that

$$dy = \frac{T}{T_e} dS$$

In that case,

$$\theta = \int_0^{\delta} \frac{\rho u}{\rho_e U_e} \left(1 - \frac{u}{U_e}\right) dy =$$

$$= \int_0^{\delta_s} \frac{\rho T}{\rho_e T_e} \frac{u}{U_e} \left(1 - \frac{u}{U_e}\right) dS$$

and since $\frac{PT}{P_e T_e} = \frac{P}{P_e} = 1$;

$$\theta = \int_0^{\delta_s} \frac{u}{U_e}\left(1 - \frac{u}{U_e}\right) dS = \theta_s \qquad (3.8)$$

where the subscript s denotes incompressible variables. Also,

$$(\delta - \delta^*) = \int_0^{\delta} \frac{\rho u}{\rho_e U_e}\, dy = \int_0^{\delta_s} \frac{u}{U_e}\, dS = (\delta_s - \delta_s^*) \qquad (3.9)$$

and

$$\delta = \int_0^{\delta} dy = \int_0^{\delta_s} \frac{T}{T_e}\, dS \qquad (3.10)$$

Substituting for (T/T_e) in (3.10) from the energy equation (3.1),

$$\delta = \int_0^{\delta_s} \left[1 + \frac{\gamma - 1}{2} M_e^2 \left(1 - \frac{u^2}{U_e^2}\right)\right] dS$$

or

$$\delta = \delta_s + \frac{\gamma - 1}{2} M_e^2 \int_0^{\delta_s} \left[\left(1 - \frac{u}{U_e}\right) + \frac{u}{U_e}\left(1 - \frac{u}{U_e}\right)\right] dS$$

$$\delta = \delta_s + \frac{\gamma - 1}{2} M_e^2 (\theta_s + \delta_s^*) \qquad (3.11)$$

The first and second derivatives of the velocity at the surface are transformed as follows:

$$\left(\frac{\partial u}{\partial y}\right)_{y=0} = \left(\frac{\partial u}{\partial S}\,\frac{\partial S}{\partial y}\right)_{S=0} = \frac{T_e}{T_{o_2}}\left(\frac{\partial u}{\partial S}\right)_{S=0} \tag{3.12}$$

and

$$\left(\frac{\partial^2 u}{\partial y^2}\right)_{y=0} = \left[\frac{\partial}{\partial S}\left(\frac{\partial u}{\partial S}\,\frac{T_e}{T}\right)_{S=0}\frac{\partial S}{\partial y}\right]_{S=0} = \left(\frac{T_e}{T_{o_2}}\right)^2\left(\frac{\partial^2 u}{\partial S^2}\right)_{S=0} \tag{3.13}$$

The transformed momentum equation and boundary condition will therefore become

$$-\frac{d}{dx}\left[\rho_e U_e^2 \theta_s\right] + \rho_e U_e \frac{dU_e}{dx}\left(\delta_s - \delta_s^*\right) + \\ + \frac{dp_e}{dx}\left[\delta_s + \frac{\gamma-1}{2}M_e^2\left(\theta_s + \delta_s^*\right)\right] = -\mu_{o_2}\left(\frac{T_e}{T_{o_2}}\right)\left(\frac{\partial u}{\partial S}\right)_{S=0} \tag{3.14}$$

and

$$\frac{dp_e}{dx} = \mu_{o_2}\left(\frac{T_e}{T_{o_2}}\right)^2\left(\frac{\partial^2 u}{\partial S^2}\right)_{S=0} \tag{3.15}$$

3.5 Thwaites' Results for Incompressible Boundary Layers

A brief discussion of Thwaites' approximate solution for incompressible boundary layers with arbitrary pressure gradients is presented in this section. Thwaites' approach

is then used to derive a method for obtaining the distribution of a new boundary layer parameter needed in the solution of the non-isentropic equations.

In Ref. 5, Thwaites attempts to find some universal relationship between the first and second derivatives of the velocity at the surface for one-parameter families of solutions. He defines non-dimensional parameters

$$m_s = \frac{\theta_s^2}{U_e}\left(\frac{\partial^2 u}{\partial s^2}\right)_{s=0} \tag{3.16a}$$

$$l_s = \frac{\theta_s}{U_e}\left(\frac{\partial u}{\partial s}\right)_{s=0} \tag{3.16b}$$

$$H_s = \frac{\delta_s^*}{\theta_s} \tag{3.16c}$$

The parameter m_s is related to the pressure gradient through the boundary condition at the surface, and it may therefore be determined if this pressure gradient is known. Thwaites then proceeds to plot the parameters l_s and H_s as functions of m_s for several special forms of the pressure gradient, for which the boundary layer equations have been solved exactly. He notes that these curves lie fairly close together, particularly for the case of negative pressure gradients (negative m_s). By fitting the best average curve to the $l_s - m_s$ and $H_s - m_s$ plots for the different exact solutions, he finds a fairly universal relationship between these parameters, which he presents in

tabular form in Table I of his paper. For the solution of an isentropic boundary layer (for which Bernoulli's equation may be used), a combination of the previous parameters in the form

$$L_s = 2\left[(H_s + 2)m_s + l_s\right] \tag{3.17}$$

is important, and Thwaites shows that the parameter $[L_s(m_s)]$ lies within close limits for all the exact solutions throughout the entire range of m_s . Furthermore, the average variation of L_s with m_s is very close to linear, and Thwaites then assumes a universal relationship.

$$L_s = .45 + 6m_s \tag{3.18}$$

With Thwaites' definitions of the incompressible parameters, Eqs. (3.12) and (3.13) may be written as

$$-\frac{d}{dx}\left[\rho_e U_e^2 \theta_s\right] + \rho_e U_e \theta_s \left(\frac{\delta_s - \delta_s^*}{\theta_s}\right) + $$

$$+ \frac{dp_e}{dx}\left[\delta_s + \frac{\gamma-1}{2} M_e^2 (\theta_s + \delta_s^*)\right] = -\mu_{o_2}\left(\frac{T_e}{T_{o_2}}\right)\frac{U_e}{\theta_s} l_s \tag{3.19}$$

and

$$\frac{dp_e}{dx} = \mu_{o_2}\left(\frac{T_e}{T_{o_2}}\right)^2 \frac{U_e}{\theta_s^2} m_s \tag{3.20}$$

As will be seen later, a new non-dimensional parameter appears in the solution of the non-isentropic case. This is the difference between boundary layer and displacement thicknesses, divided by the momentum thickness. This parameter has been shown in Section 3.4 to be independent of the coordinate transformation. That is,

$$K \equiv \frac{\delta - \delta^*}{\theta} = \frac{\delta_s - \delta_s^*}{\theta_s} \equiv K_s$$

It is desirable to obtain some relationship between this parameter K_s and the parameter m_s. This has been done following an approach analogous to Thwaites'. K_s was plotted as a function of m_s for three know cases*: The Faulkner-Skan[11] solution, the Karman-Pohlhausen[8] solution and the Howarth[8] solution for pressure gradients of the form $p_e = a + b x^m$. The results appear plotted in Figure 14. It may be seen that they lie fairly close together. From Figure 14, a simple linear "universal" relationship was fitted:

$$K_s = -1.60\, m_s + 6.2 \qquad (3.21)$$

---

* δ_s was assumed to be the height at which $(u/U_e) = .999$.

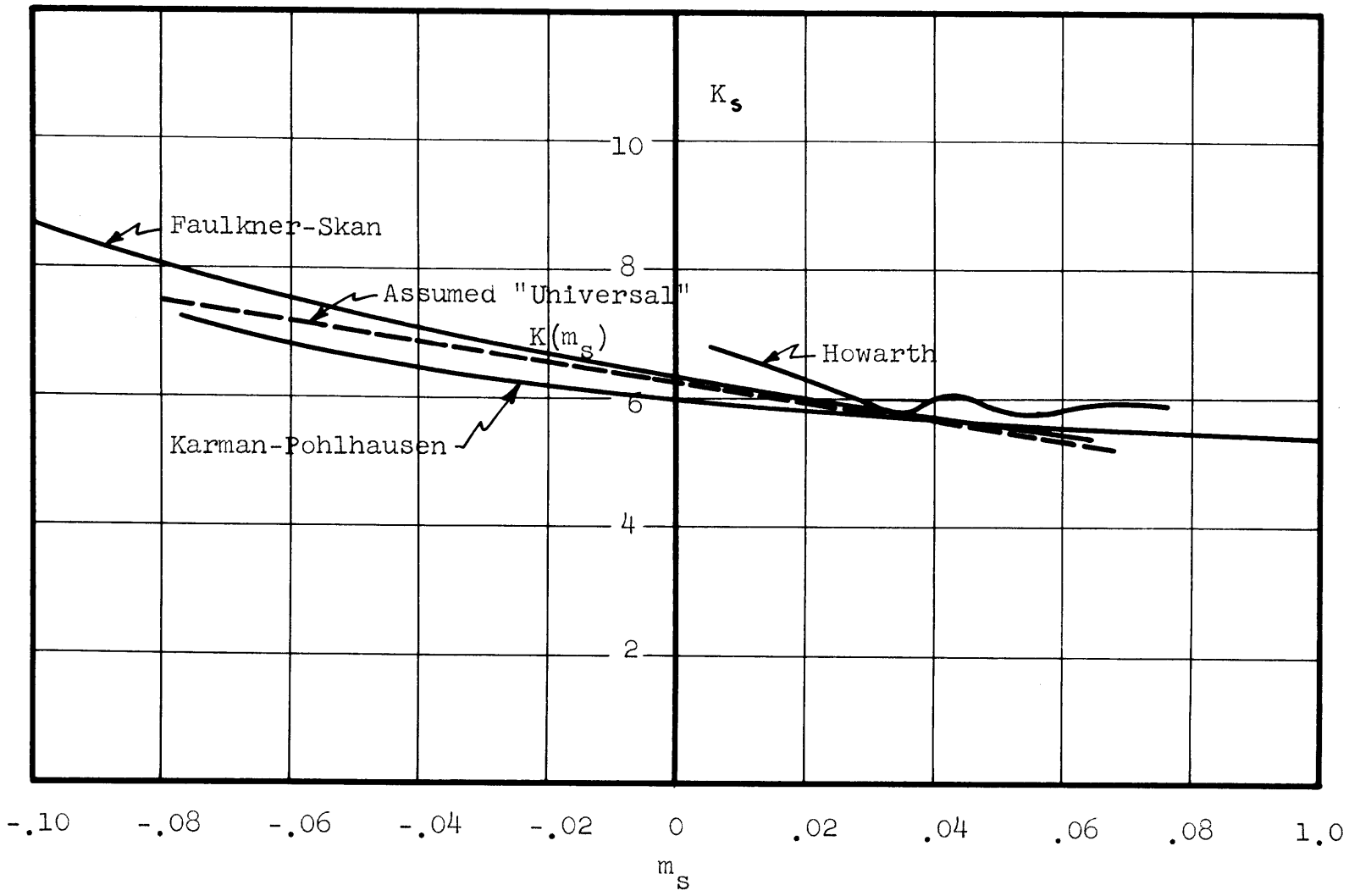

Figure 14 Variation of K_s with m_s.

3.6 Shock-Boundary Layer Continuity Equation

In Section 3.1 it was suggested that the variation in boundary layer edge conditions with x could be obtained by relating x to the height y_1 at which the streamline intersecting the edge of the boundary layer at x intersects the curved shock. This may be done by writing a mass-balance equation between a station ahead of the shock and a station at x (see sketch in Figure 13). Since the mass flow in the boundary layer is equal to $\rho_e U_e (\delta - \delta^*)$, this relationship will be —— for unit length along the span :

$$\rho_1 U_1 y_1 = (\delta - \delta^*) \rho_e U_e$$

or

$$\rho_1 U_1 y_1 = \rho_e U_e K\Theta = \rho_e U_e K_s \Theta_s \qquad (3.22)$$

3.7 Shock Shape

As stated in the Introduction, a hyperbolic shock shape following the results of Love (Ref. 3) has been assumed. Figure 15 illustrates the important variables and parameters in Love's simplified calculation of the shock shape. Figure 15 is a reproduction of Figure 9 in Love's paper, with some of the letters changed to avoid confusion with other variables being used in the present discussion.

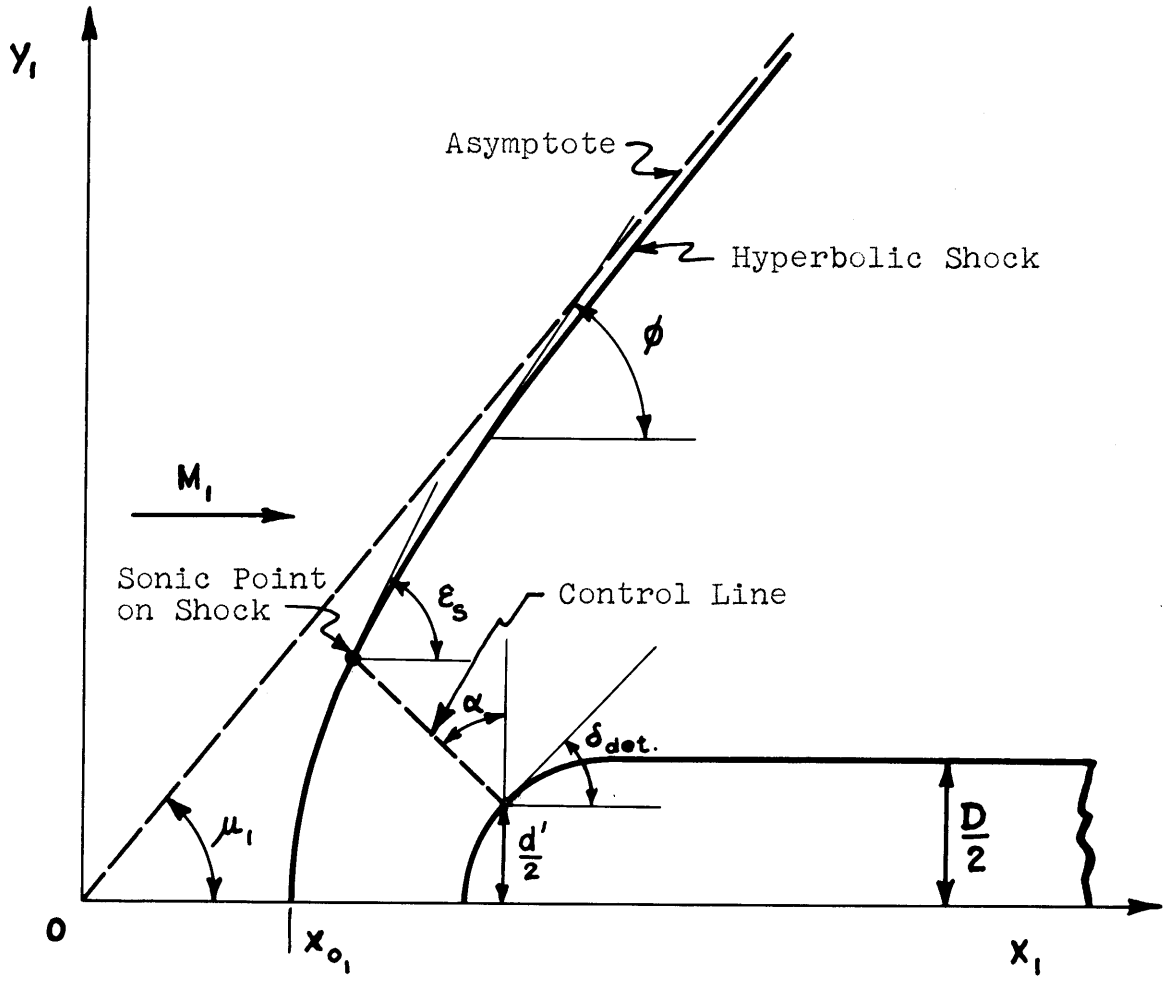

d' : Diameter at which body has a slope equal to tan δ_{det}

δ_{det} : Angle at which shock detachment first occurs for a wedge in a stream at M_1

μ_1 : Mach angle corresponding to M_1

ε_s : Angle at which the Mach number behind the shock is equal to unity

ϕ : Local shock inclination angle

Figure 15 Shock Shape.

The assumption of a hyperbolic shock shape which is asymptotic to a Mach line yields an expression of the form

$$\frac{Y_1}{D} = \frac{1}{\sqrt{M_1^2 - 1}} \sqrt{\left(\frac{x_1}{D}\right)^2 - \left(\frac{x_0}{D}\right)^2} \qquad (3.23)$$

It is necessary to evaluate the quantity (x_0/D), which for semicircular noses is related to (x_0/d') by

$$\frac{x_0}{D} = \frac{x_0}{d'} \cos \delta_{det.} \qquad (3.24)$$

Love evaluates the quantity (x_0/d') by a method which is essentially based on a large number of experimental results obtained at different Mach numbers. He presents an empirical graph of the inclination angle α of a "control line" which is representative of, though not equal to, the sonic line. He then uses trigonometric relationships derived by Moeckel, to relate α to the quantity (x_0/d'). The relationship is

$$\frac{x_0}{d'} = \frac{\sqrt{M_1^2 - 1}\sqrt{(M_1^2 - 1)\tan^2 \varepsilon_s - 1}\left[\frac{x'}{d'} + \frac{\tan \alpha}{2}\right]}{(M_1^2 - 1)\tan \varepsilon_s - \sqrt{M_1^2 - 1}\sqrt{(M_1^2 - 1)\tan^2 \varepsilon_s - 1} + \tan \alpha} \qquad (3.25)$$

where (x'/d') is the shock-standoff distance, which Love assumes to be simply given by

$$\frac{x'}{d'} = .5C \cot \delta_{det.} \tag{3.26}$$

The coefficient C is also obtained from experimental results. It will be equal to unity if the shock is attached, and have a value close to unity when the shock is detached. Love's Figure 2 gives the variation of this coefficient with free stream Mach number.

For the purposes of the present analysis, it will be useful to relate the coordinate y_1 to the local shock inclination angle ϕ. This may be done as follows:

From Eq. (3.23)

$$\frac{dy_1}{dx_1} = \tan \phi = \frac{x_1/D}{\sqrt{M_1^2-1}\sqrt{\left(\frac{x_1}{D}\right)^2 - \left(\frac{x_0}{D}\right)^2}}$$

Solving for x_1/D,

$$\left(\frac{x_1}{D}\right)^2 = \frac{(M_1^2-1)\tan^2\phi \left(x_0/D\right)^2}{(M_1^2-1)\tan^2\phi - 1}$$

Finally, substituting for $(x_1/D)^2$ in (3.23) and solving

for ϕ

$$\phi = \tan^{-1}\left[\frac{1}{\sqrt{M_1^2-1}}\sqrt{\frac{(x_o/D)^2}{(M_1^2-1)\left(\frac{Y_1}{D}\right)^2}+1}\right] \qquad (3.27)$$

For the particular free-stream Mach number being considered ($M_1 = 7.6$),

$$\delta_{det.} = 43.5^\circ$$
$$\varepsilon_s = 66^\circ$$
$$M_1^2-1 = 56.76$$

($\delta_{det.}$ and ε_s have been obtained from the NACA isentropic flow charts and tables (Ref. 10)).

Love's Figure 2 yields a numerical value for C of .951, at $M_1 = 7.6$. (x'/d') may therefore be calculated. In order to obtain α , it was necessary to extrapolate Love's graph for the experimental variation of α with M_1 . This extrapolated distribution is shown in Fig. 16. α for $M_1 = 7.6$ is then found to have a numerical value of 76.5°. (x_o/d') may then be evaluated, and finally (x_o/D) may be found to have a value of 57.3. Substituting then into (3.25), the expression for ϕ becomes

$$\phi = \tan^{-1}\left[.1328\sqrt{\frac{57.845}{(Y_1/D)^2}+1}\right] \qquad (3.28)$$

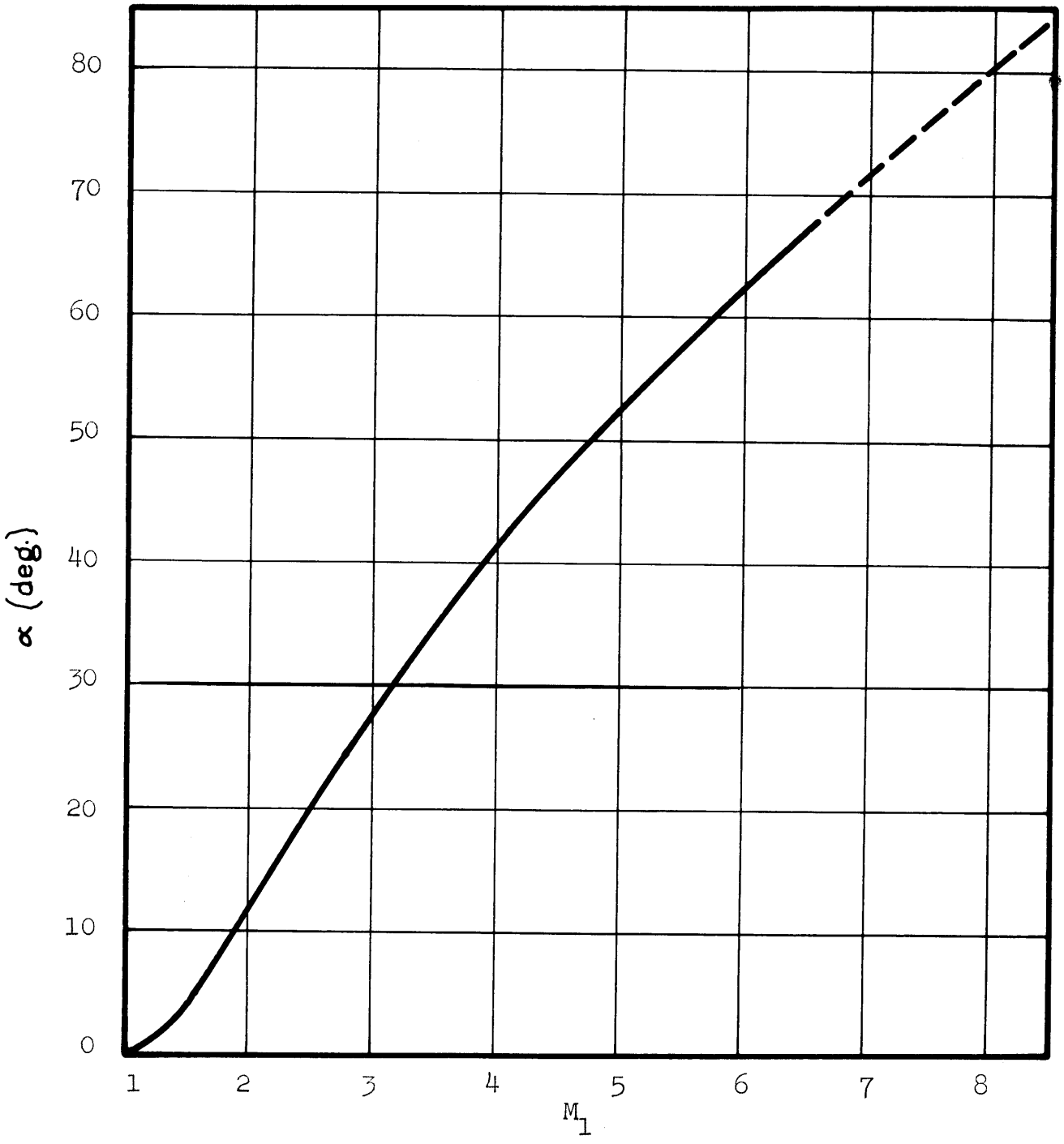

Figure 16 Variation of α with M_1.

CHAPTER 4

CONSTANT PRESSURE-VARIABLE ENTROPY CASE

4.1 The results described in Chapter 2 have pointed out the possibility of replacing the actual isentropic blunt plate by a fictitious isentropic plate with constant static pressure. The results in both cases were shown to be approximately equivalent, especially at the higher values of ξ . This approximation will now be carried into the non-isentropic region, because the assumption of constant static pressure considerably simplifies the analysis. For the constant-pressure, variable-entropy (C.P.-V.E.) case, therefore,

$$\frac{dp_e}{dx} = 0$$

This means that the Thwaites parameter m_s will therefore be zero everywhere. All other parameters which are functions of m_s , i.e., l_s , H_s and K_s , will therefore remain constant at the values corresponding to $m_s = 0$. It should be noted, however, that since Bernoulli's equation

no longer applies, dU_e/dx will in general not be equal to zero.

4.2 Solution of Momentum Equation

For constant static pressure, the transformed momentum equation (3.19) will reduce to

$$-\frac{d}{dx}(\rho_e U_e^2 \theta_s) + \rho_e U_e \theta_s \left(\frac{\delta_s - \delta_s^*}{\theta_s}\right)\frac{dU_e}{dx} = -\mu_{o_2}\left(\frac{T_e}{T_{o_2}}\right)\frac{U_e}{\theta_s} l_s \quad (4.1)$$

and the boundary condition at the surface yields

$$\frac{dp_e}{dx} = \mu_{o_2}\left(\frac{T_e}{T_{o_2}}\right)^2 \frac{U_e}{\theta_s^2} m_s \ ,$$

or

$$m_s = 0$$

These equations hold, of course, under the assumptions of $Pr = 1$ and $q_w = 0$ for which (3.19) was derived.

Equation (4.1) will be solved using the shock-boundary layer continuity condition (3.22) to obtain a relationship between y_1 and the boundary layer edge conditions. Equation (3.22) may be written

$$\frac{\rho_1 U_1}{K_s} y_1 = \rho_e U_e \theta_s$$

and substituting for $\rho_e U_e \theta_s$ into (4.1),

$$\frac{\rho_1 U_1}{K_s}\frac{d}{dx}(U_e y_1) - \rho_1 U_1 y_1 \frac{dU_e}{dx} = \frac{\mu_{o_2} l_s K_s}{\rho_1 U_1}\left(\frac{T_e}{T_{o_2}}\right)\rho_e U_e^2 \frac{1}{y_1}$$

Multiplying through by $\frac{2K_s}{\rho_1 U_1}$ and expanding the first derivative,

$$2U_e \frac{dy_1}{dx} + 2(1-K_s) y_1 \frac{dU_e}{dx} = \frac{2\mu_{o_2} l_s K_s^2}{\rho_1 U_1}\left(\frac{T_e}{T_{o_2}}\right)\frac{\rho_e U_e^2}{\rho_1 U_1}\frac{1}{y_1}$$

and multiplying through by (y_1/U_e):

$$\frac{dy_1^2}{dx} + 2(1-K_s) y_1^2 \frac{1}{U_e}\frac{dU_e}{dx} = \frac{2\mu_{o_2}}{\rho_1 U_1} l_s K_s^2 \frac{\rho_e U_e}{\rho_1 U_1}\left(\frac{T_e}{T_{o_2}}\right) \tag{4.1a}$$

Now

$$\left(\frac{U_e}{a_o}\right)^2 = M_e^2 \frac{T_e}{T_{o_2}} = M_e^2\left[1 + \frac{\gamma-1}{2} M_e^2\right]^{-1} \tag{4.2}$$

using the iso-energetic flow equation for the temperature ratio. Taking the logarithm of both sides, (4.2) becomes

$$2\ln U_e - 2\ln a_o = 2\ln M_e - \ln\left[1 + \frac{\gamma-1}{2} M_e^2\right]$$

Differentiating implicity and collecting terms,

$$\frac{1}{U_e}\frac{dU_e}{dx} = \frac{dM_e/dx}{M_e\left[1+\frac{\gamma-1}{2}M_e^2\right]}$$

Substituting into (4.1a),

$$\frac{d}{d\xi}\left(Y_1/D\right)^2 + \left(Y_1/D\right)^2\left[\frac{2(1-K_s)}{M_e\left(1+\frac{\gamma-1}{2}M_e^2\right)}\frac{dM_e}{d\xi}\right] = \frac{2\mu_{o_2}}{D\rho_1 U_1}\, l_s K_s^2 \frac{\rho_e U_e}{\rho_1 U_1}\frac{T_e}{T_{o_2}} \qquad (4.3)$$

where $\xi = x/D$ has been substituted for x.

The right-hand side of Eq. (4.3) may be modified to simplify calculations as follows:

$$\frac{2\, l_s K_s^2}{Re_{D_2}}\frac{a_{o_2}\rho_{o_2}}{\rho_1 M_1 a_1}\frac{\rho_e}{\rho_1}\frac{M_e a_e}{M_1 a_1}\frac{T_e}{T_{o_2}} = \left[\frac{2\, l_s K_s^2}{Re_{D_2}}\frac{1}{M_1^2}\left(\frac{\rho_{o_2}}{\rho_1}\right)\left(\frac{T_1}{T_{o_2}}\right)\right] M_e\left(\frac{T_e}{T_{o_2}}\right)^{1/2} \qquad (4.3a)$$

where $Re_{D_2} = \left(a_{o_2}\rho_{o_2}D/\mu_{o_2}\right)$ is the stagnation Reynolds number based on conditions at the nose of the plate.

The bracketed quantity in (4.3a) will be a constant for any given free-stream conditions, and will be denoted by B. Equation (4.3) may therefore be written as

$$\frac{d}{d\xi}\left(Y_1/D\right)^2 + \left(Y_1/D\right)^2\left[\frac{2(1-K_s)}{M_e\left(1+\frac{\gamma-1}{2}M_e^2\right)}\frac{dM_e}{d\xi}\right] = B\, M_e\left(\frac{T_e}{T_{o_2}}\right)^{1/2} \qquad (4.4)$$

Equation (4.4) is an ordinary first order differential equation in the variable $\left[Y_{1}/D(\xi)\right]^{2}$, with coefficients which are functions of ξ . It may be solved exactly, and the solution (Ref. 12) is given by

$$\eta = e^{-\int_{0}^{\xi} P(\xi)\,d\xi} \int_{0}^{\xi} e^{\int_{0}^{\xi} P(\xi)\,d\xi} Q(\xi)\,d\xi + \text{int. constant} \tag{4.5}$$

where

$$\eta = \left(Y_{1}/D\right)^{2}$$

$$P(\xi) = \frac{2(1-K_{s})}{M_{e}\left(1+\frac{\gamma-1}{2}M_{e}^{2}\right)}\frac{dM_{e}}{d\xi}$$

$$Q(\xi) = B M_{e}\left(\frac{T_{e}}{T_{o_2}}\right)^{1/2}$$

The integration constant will be zero because

$$\eta(0) = 0$$

Carrying out the integration of $P(\xi)$, it is possible to obtain that

$$\int_{0}^{\xi} P(\xi)\,d\xi = (1-K_{s})\ln\left[\frac{T_{e}}{T_{o_2}}M_{e}^{2}\cdot\frac{T_{o_2}}{T_{e_2}}\frac{1}{M_{e_2}^{2}}\right]$$

Equation (4.5) then becomes

$$\eta = B\left[\frac{T_{e}}{T_{o_2}}M_{e}^{2}\right]^{-(1-K_{s})}\int_{0}^{\xi}\left[\frac{T_{e}}{T_{o_2}}M_{e}^{2}\right]^{(1-K_{s})}\left[\frac{T_{e}}{T_{o_2}}M_{e}^{2}\right]^{1/2}d\xi$$

$$\eta = B\left[\frac{T_e}{T_{o_2}} M_e^2\right]^{(K_s-1)} \int_0^{\xi} \left[\frac{T_e}{T_{o_2}} M_e^2\right]^{\frac{3-2K_s}{2}} d\xi \qquad (4.6)$$

With given boundary layer edge conditions, Eq. (4.6) yields the shock intersection point of streamlines intersecting the boundary layer at $\delta(\xi)$. By assuming an edge Mach number distribution, it is then possible to calculate the shock intersection parameter η as a function of ξ . With the assumed hyperbolic shock shape it is then possible to obtain the local shock inclination angle ϕ as a function of ξ . (See Fig. 17.)

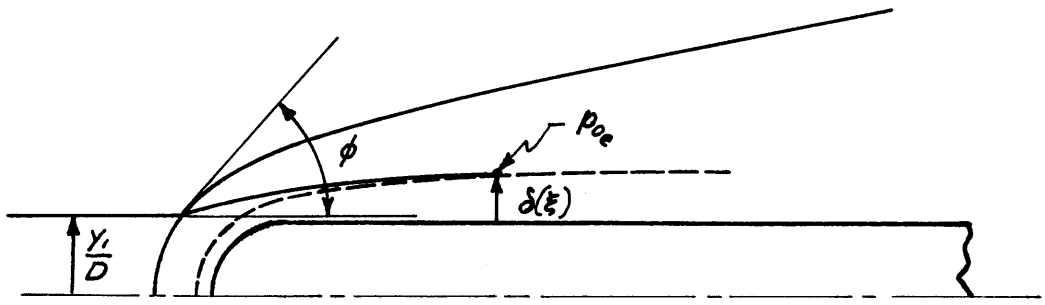

Figure 17.

Using oblique shock relationships the stagnation pressure behind the shock can be obtained, which is equal to the local edge stagnation pressure p_{o_e} , at ξ . The ratio p_e/p_{o_e} will then yield a new edge Mach number distribution through the isentropic relationship between pressure ratio and Mach number

$$\frac{p_e}{p_{o_e}} = \left[1 + \frac{\gamma-1}{2} M_e^2\right]^{-\frac{\gamma}{\gamma-1}}$$

This isentropic relationship may be used in this case because the entropy along the streamline in Fig. 17 is constant. With the new edge Mach number distribution, a new $\eta(\xi)$ may be calculated by using Eq. (4.6), and the iterative procedure may be continued until the edge conditions converge to some final distribution.

When the final edge conditions have been calculated, the momentum thickness may be obtained from the shock-boundary layer mass balance equation, which has been seen to be

$$\frac{\rho U_1}{\rho_e U_e} \frac{1}{K_s} \sqrt{\eta} = \frac{\theta}{D} \qquad (4.7)$$

From the momentum thickness, the displacement thickness and displacement thickness slopes may be calculated; and finally, the boundary layer pressure influence coefficient obtained from the Prandtl-Meyer expansion relationship.

4.3 Calculations and Results

4.3.1 Calculation of Edge Conditions

The constants in Eq. (4.6) must be evaluated before proceeding with calculations. The constant

$$K_s = K = \frac{\delta - \delta^*}{\theta} = \left(\frac{\delta - \delta^*}{\theta}\right)_s$$

is computed from the Blasius solution to the flat-plate problem, and is found to have a numerical value of 6.43*. Table II in Ref. 8 has been used, choosing as δ the point where $(u/U_e) = .99898$. The constant B has been calculated from the NACA Compressible Flow Tables (Ref. 10) and is found to have a numerical value of 1.837×10^{-3}. Equation (4.6) then becomes

$$\eta = 1.837 \times 10^{-3} \left[\frac{T_e}{T_{o_2}} M_e^2\right]^{5.43} \int_0^{\xi} \left[\frac{T_e}{T_{o_2}} M_e^2\right]^{-4.93} d\xi \qquad (4.8)$$

For the first iteration the edge conditions are assumed to be those for the isentropic case, i.e.,

$$M_e = 3.4868 = \text{constant}$$

---

* A value $K(0) = 6.43$ from the Blasius solution was assumed rather than the value given by the "universal" relationship $K_s = -1.6 m_s + 6.2$, because the Blasius case is exact.

Once η has been calculated from Eq. (4.8), the shock inclination angle ϕ at η can be obtained from Eq. (3.28). Three distributions of ϕ were calculated following the iterative scheme described above and the results are shown in Figure 18. $\phi^{(3)}$ lies close enough to $\phi^{(2)}$, so that it was not necessary to compute any further approximations. The final shock angle distribution $\phi^{(3)}$ yields the final edge Mach number distribution $M_e^{(4)}$, which is shown in Figure 19, together with the Mach number distributions found for the other iterations. It is evident that the edge Mach number varies between the isentropic constant-pressure (C.P.-C.E.) value of 3.487, and the free stream value of 7.6.

4.3.2 Calculation of Momentum Thickness

With the final edge Mach number distribution $M_e^{(4)}$, Eq. (4.7), transformed to

$$\frac{\theta}{D} = \frac{C}{M_e}\sqrt{\frac{T_e}{T_{o_2}}\eta^{(4)}} \tag{4.9}$$

where

$$C = \frac{M_1}{K_S}\sqrt{\frac{T_{o_1}}{T_1}} = 4.1873$$

was used to compute the momentum thickness distribution which appears in Fig. 20. In Fig. 20, the momentum thickness is seen to vary between those of an isentropic constant pressure blunt plate (C.P.-C.E.) and the isentropic, sharp plate (S.P.)

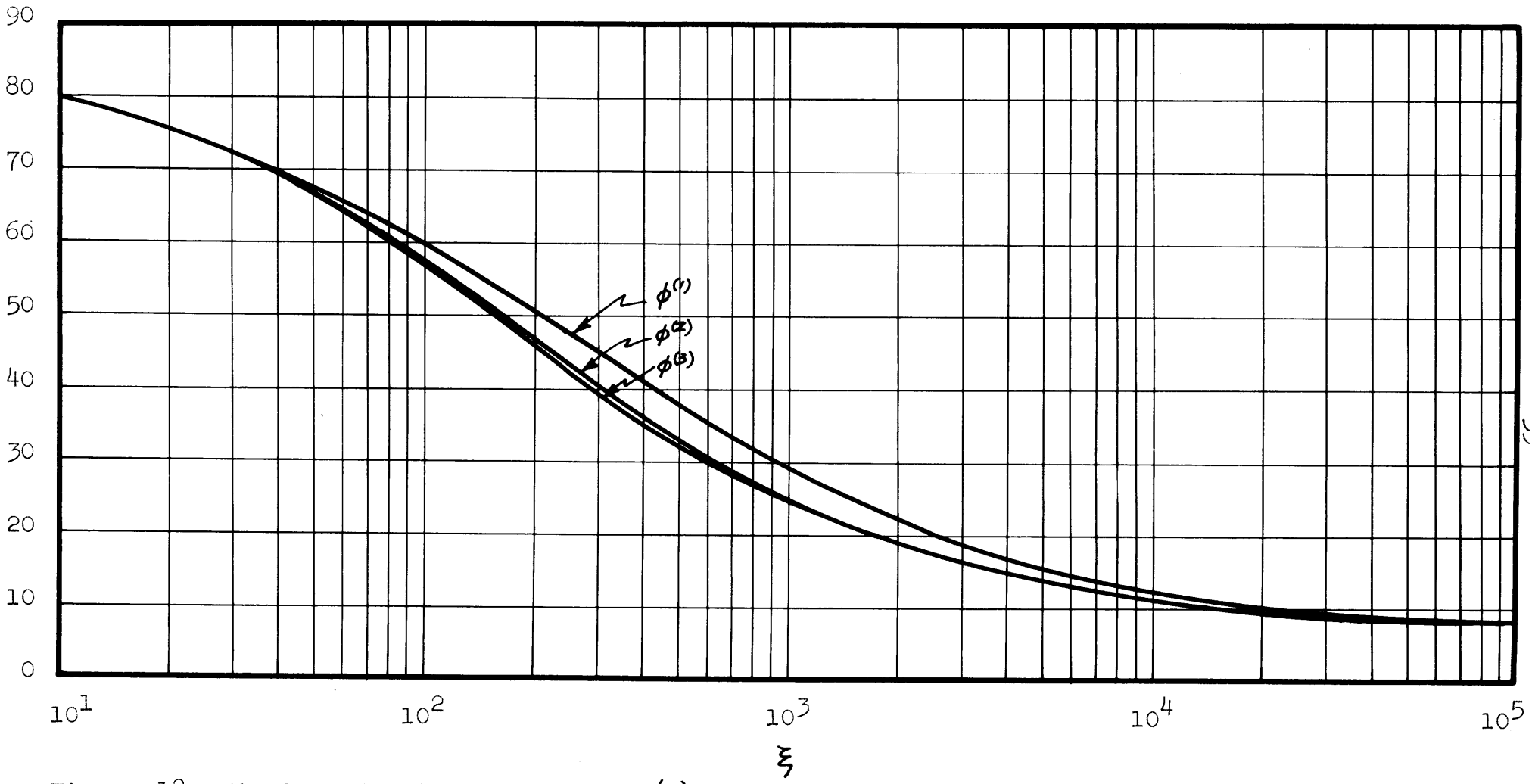

Figure 18 Shock Inclination Angle at $\eta(\xi)$

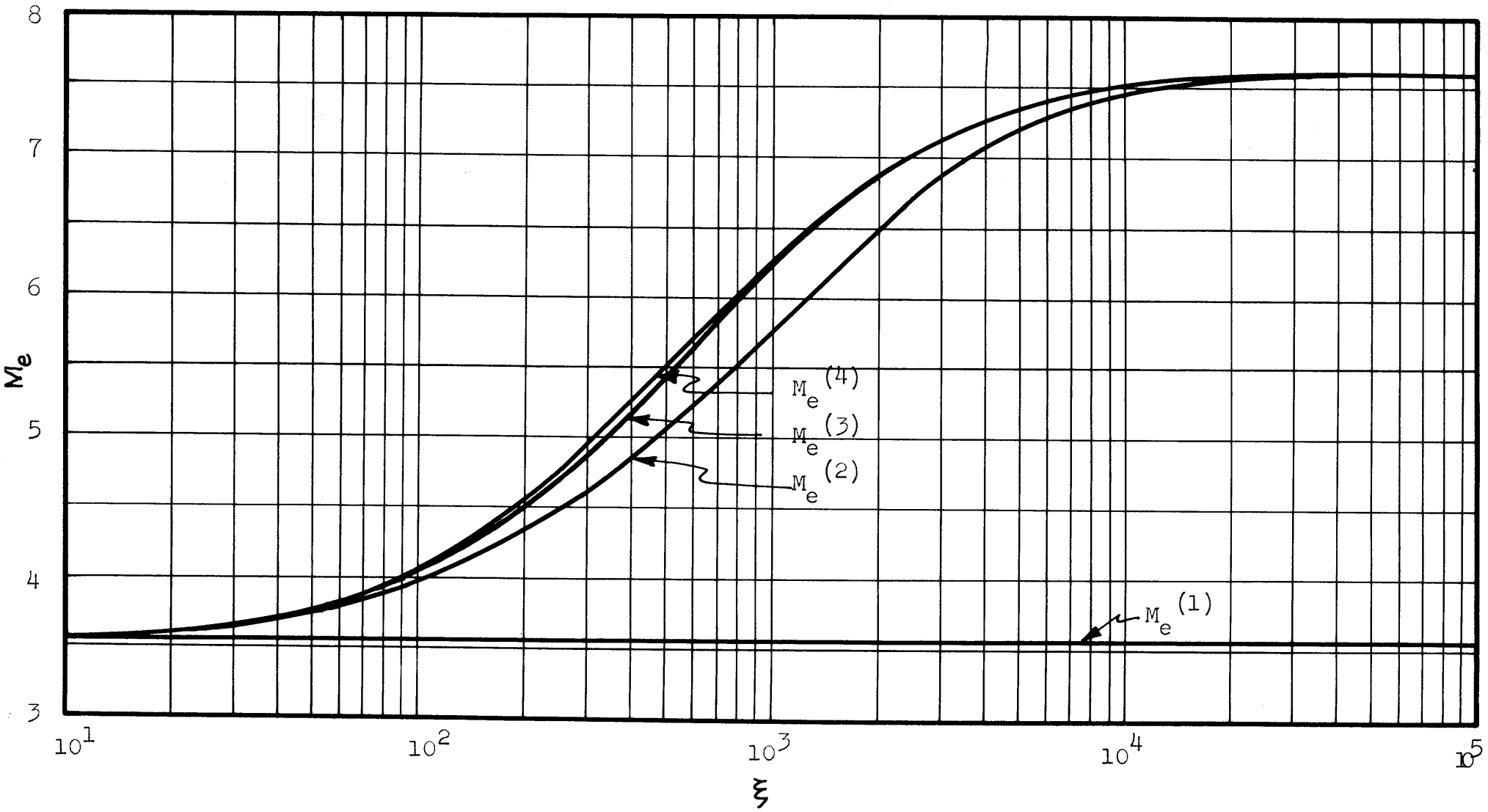

Figure 19 Edge Mach Number Distribution.

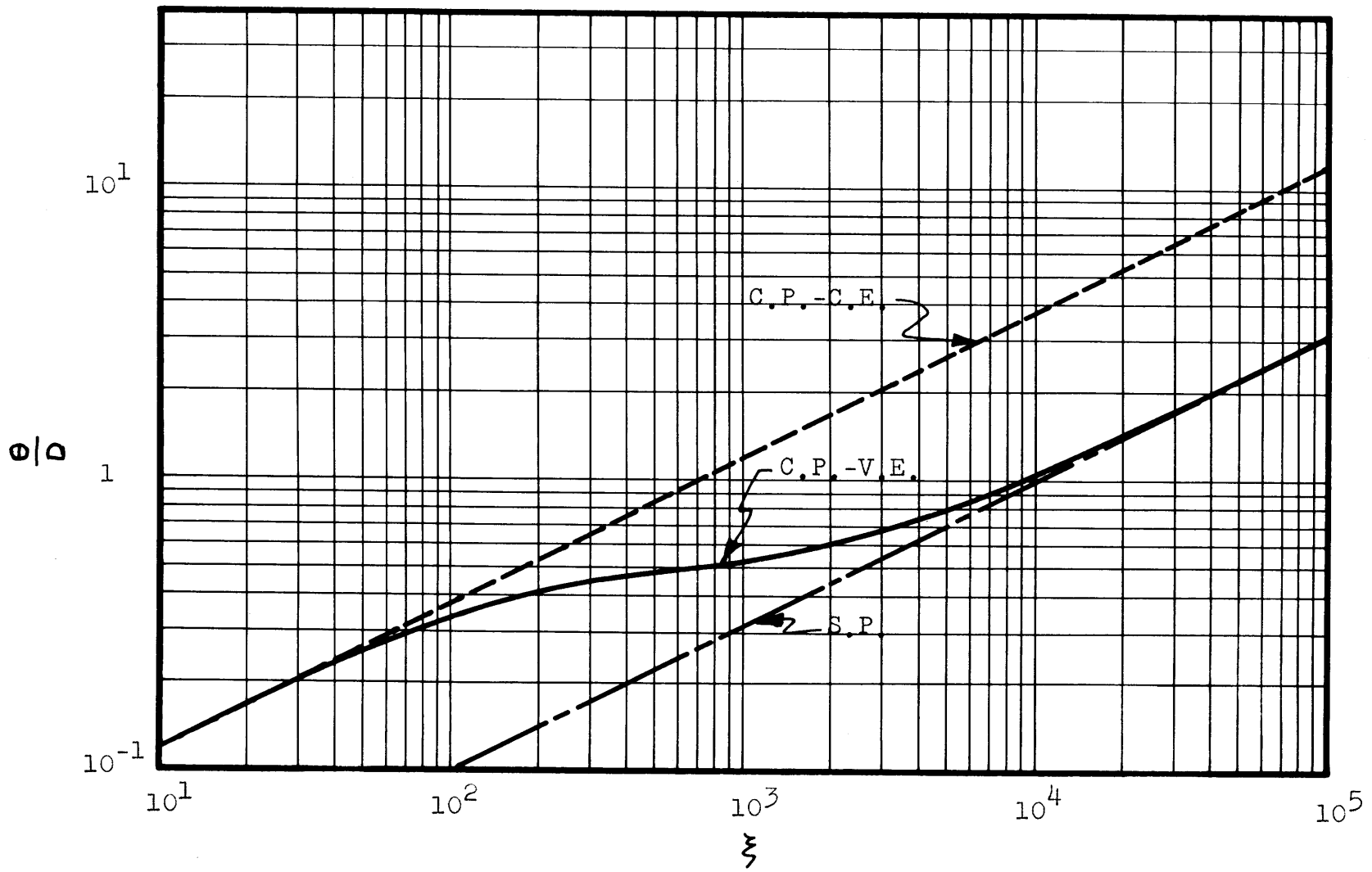

Figure 20 Distribution of Momentum Thickness.

4.3.3 Calculation of Displacement Thickness

For the non-dimensional incompressible case, the displacement thickness is given by - following Thwaites[5] -

$$\left(\frac{\delta_s^*}{D}\right) = H_s\left(\frac{\theta_s}{D}\right)$$

where H_s can be obtained from Thwaites' Table I. For the case of $m_s = 0$, which corresponds to the constant static pressure assumption, H_s has a numerical value of 2.61.

The compressible displacement thickness may be obtained from a similar expression

$$\left(\frac{\delta^*}{D}\right) = H\left(\frac{\theta}{D}\right) = H\left(\frac{\theta_s}{D}\right) \qquad (4.10)$$

provided an equivalence between the compressible parameter H and the incompressible parameter H_s can be found. This relationship is obtained as follows:

By definition, the compressible displacement thickness is given by

$$\delta^* = \int_0^{\delta}\left(1 - \frac{\rho u}{\rho_e U_e}\right) dy$$

with the Howarth transformation

$$dy = \frac{T_e}{T} dS ,$$

$$\delta^* = \int_0^{\delta_s} \left(\frac{T}{T_e} - \frac{u}{U_e} \right) dS \qquad (4.11)$$

From the energy equation for the case of $Pr = 1$ and zero heat transfer at the surface,

$$\frac{T}{T_e} = 1 + \frac{\gamma - 1}{2} M_e^2 \left(1 - \frac{u^2}{U_e^2} \right)$$

Substituting into Eq. (4.11), collecting terms and using the definitions for the incompressible momentum and displacement thicknesses,

$$\delta^* = \delta_s^* + \frac{\gamma - 1}{2} M_e^2 \left(\theta_s + \delta_s^* \right)$$

or, since $\theta = \theta_s$,

$$\frac{\delta^*}{\theta} = H = H_s + \frac{\gamma - 1}{2} M_e^2 \left(1 + H_s \right) \qquad (4.12)$$

Writing Eq. (4.12) in terms of the temperature ratio, the non-dimensional compressible displacement thickness will finally be given by

$$\left(\frac{\delta^*}{D} \right) = \left[\frac{T_{o_2}}{T_e} \left(H_s + 1 \right) - 1 \right] \frac{\theta}{D} \qquad (4.13)$$

With the edge conditions given by $M_e^{(4)}$ in Fig. 19, Eq. (4.13) has been plotted in Fig. 21. The values of for the sharp and constant-pressure isentropic flat plates are also displayed in Fig. 21 for purposes of comparison.

4.3.4 Calculation of Displacement Thickness Slope

From Eq. (4.10), the non-dimensional displacement slope is given by

$$\frac{d(\delta^*/D)}{d\xi} = H\,\frac{d(\theta/D)}{d\xi} + \frac{\theta}{D}\,\frac{dH}{d\xi} \tag{4.14}$$

where

$$\theta/D = \frac{C}{M_e}\left[\frac{T_e}{T_{o_2}}\,\eta\right]^{1/2} \tag{4.14a}$$

$$H = H_s + \frac{\gamma-1}{2}\,M_e^2\left(H_s+1\right) \tag{4.14b}$$

The differential terms in Eq. (4.14) will be transformed until they appear as a function of a single derivative - the edge Mach number slope.

From Eq. (4.14a),

$$\frac{d(\theta/D)}{d\xi} = -\frac{\theta/D}{M_e}\,\frac{dM_e}{d\xi} + \frac{C^2}{2}\,\frac{1}{M_e^2(\theta/D)}\,\frac{d\left(\frac{T_e}{T_{o_2}}\eta\right)}{d\xi} \tag{4.15}$$

The derivative in the last term of (4.15) may be written as

$$\frac{d\left(\frac{T_e}{T_{o_2}}\,\eta\right)}{d\xi} = -(\gamma-1)\,\eta\,\frac{M_e}{(T_{o_2}/T_e)^2}\,\frac{dM_e}{d\xi} + \left(\frac{T_e}{T_{o_2}}\right)\frac{d\eta}{d\xi}$$

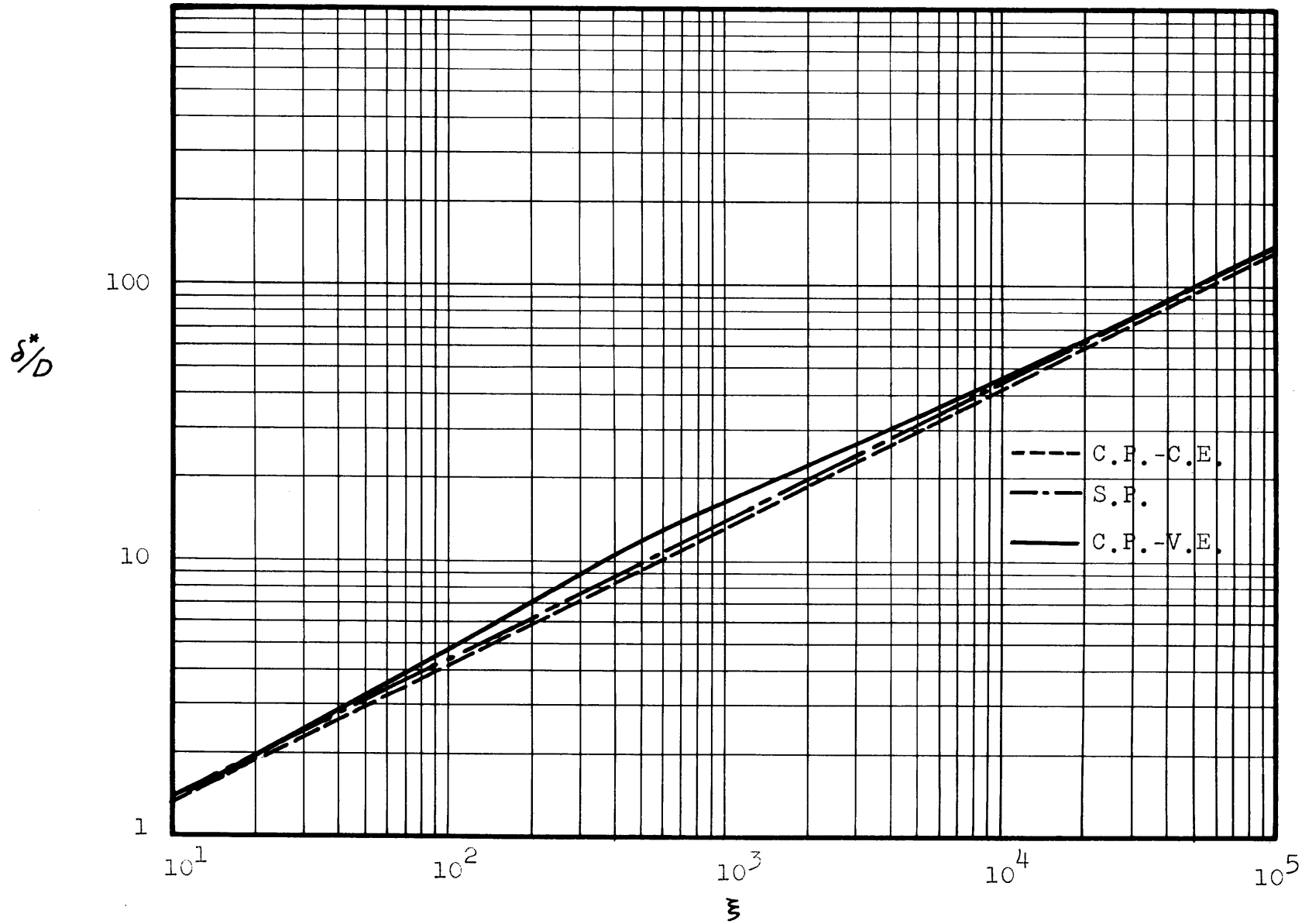

Figure 21 Displacement Thickness Distribution.

and substituting for $\frac{T_e}{T_{o_2}} \frac{d\eta}{d\xi}$ from Eq. (4.4),

$$\frac{d\left(\frac{T_e}{T_{o_2}}\eta\right)}{d\xi} = -(\gamma-1)\eta\left(\frac{T_e}{T_{o_2}}\right)^2 M_e \frac{dM_e}{d\xi} + BM_e\left(\frac{T_e}{T_{o_2}}\right)^{3/2} - 2(1-K_s)\left(\frac{T_e}{T_{o_2}}\right)^2 \eta \frac{1}{M_e}\frac{dM_e}{d\xi}$$

Combining terms,

$$\frac{d\left(\frac{T_e}{T_{o_2}}\eta\right)}{d\xi} = BM_e\left(\frac{T_e}{T_{o_2}}\right)^{3/2} - 2\eta\left(\frac{T_e}{T_{o_2}}\right)^2 \frac{1}{M_e}\frac{dM_e}{d\xi}\left[\frac{T_{o_2}}{T_e} - K\right]$$

Substituting in (4.15) and combining terms,

$$\frac{d(\theta/D)}{d\xi} = \frac{C^2 B}{2}\left(\frac{T_e}{T_{o_2}}\right)^{3/2}\frac{1}{M_e(\theta/D)} - \frac{1}{M_e}\frac{dM_e}{d\xi}\left(\frac{\theta}{D}\right)\cdot \left\{\frac{T_e}{T_{o_2}}\left[\frac{T_{o_2}}{T_e} - K\right] + 1\right\} \tag{4.16}$$

From Eq. (4.14b),

$$\frac{dH}{d\xi} = (\gamma-1)(H_s+1)M_e\frac{dM_e}{d\xi} \tag{4.17}$$

and substituting (4.16) and (4.17) into (4.14),

$$\frac{d(\delta^*/D)}{d\xi} = \frac{C^2 B}{2} H\left(\frac{T_e}{T_{o_2}}\right)^{3/2}\frac{1}{M_e(\theta/D)} - \frac{H}{M_e}\frac{dM_e}{d\xi}\left(\frac{\theta}{D}\right)\cdot \left\{\frac{T_e}{T_{o_2}}\left[\frac{T_{o_2}}{T_e} - K\right] + 1\right\} + (\gamma-1)(H_s+1)\left(\frac{\theta}{D}\right)M_e\frac{dM_e}{d\xi}$$

and collecting terms

$$\frac{d(\delta^*/D)}{d\xi} = \frac{C^2 B}{2} H \left(\frac{T_e}{T_{o_2}}\right)^{3/2} \frac{1}{M_e(\theta/D)} + \left(\frac{\theta}{D}\right) \frac{dM_e}{d\xi} \cdot$$

$$\cdot \left\{ (\gamma-1)(H_s+1) M_e + \frac{H}{M_e} \left[\frac{T_e}{T_{o_2}} \left(K - \frac{T_{o_2}}{T_e} \right) - 1 \right] \right\} \qquad (4.18)$$

Equation (4.18) has been plotted in Figure 22. The edge Mach number slope was calculated by drawing a large-scale graph of the edge Mach number distribution and fitting tangent lines at the points of interest. The displacement thickness slopes for the two isentropic plates are also displayed in Fig. 22.

4.3.5 Calculation of the Pressure Influence of the Boundary Layer

In order to calculate the pressure increment produced by the presence of the boundary layer, a Prandtl-Meyer expansion about an effective inviscid body whose local surface slope is equal to the local slope of the displacement thickness is assumed. The expression for the pressure disturbance will then be, to the first order,

$$\frac{\Delta p}{p_{o_2}} = \frac{\gamma M_e^2}{(M_e^2 - 1)^{1/2}} \left(\frac{p_e}{p_{o_2}}\right) \frac{d(\delta^*/D)}{d\xi} \qquad (4.19)$$

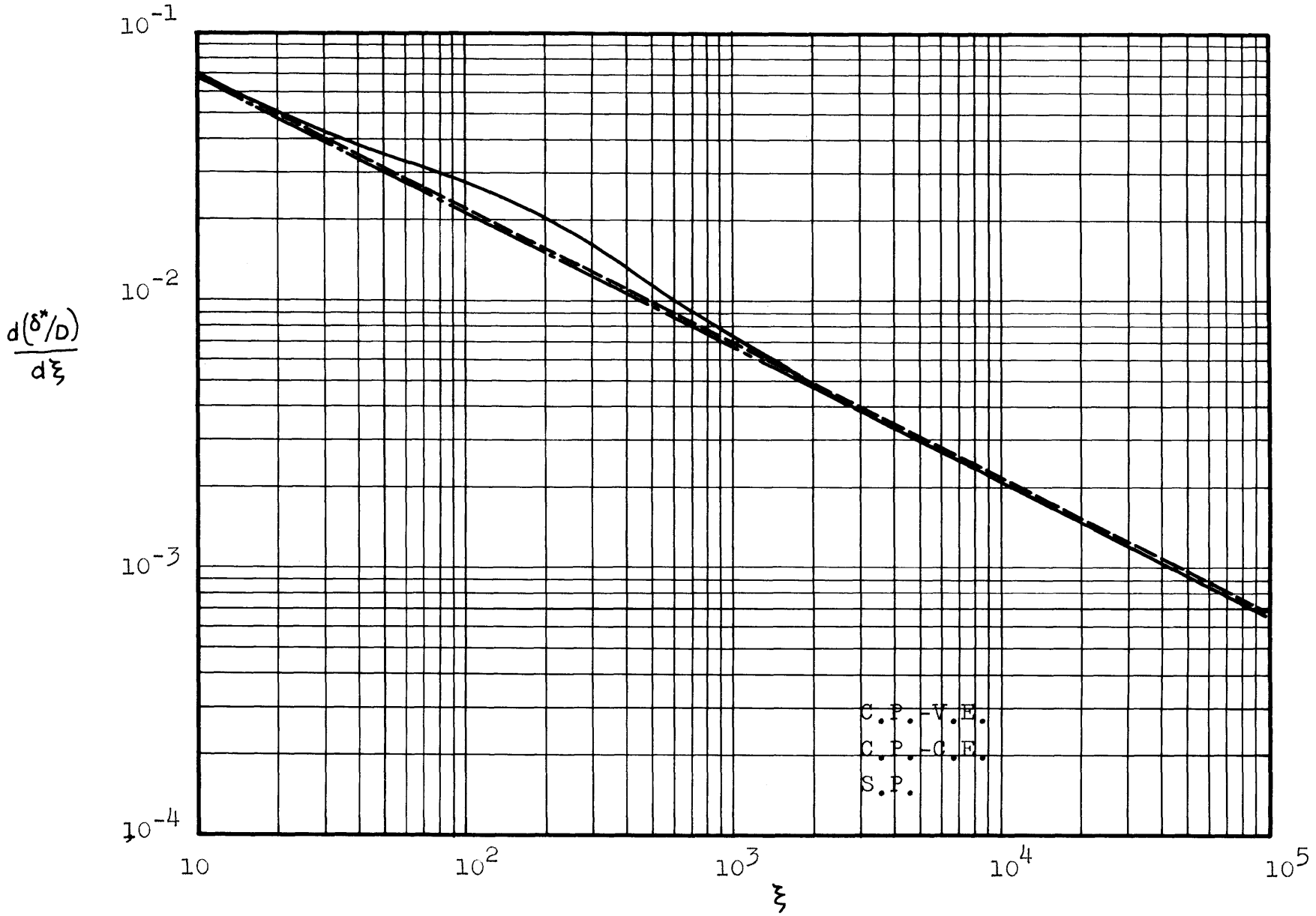

Figure 22 Distribution of Displacement Thickness Slope

With the edge Mach number and displacement thickness slope previously computed $\left(\Delta p/p_{o_2}\right)$ may be calculated. Equation (4.19) has been plotted and appears in Fig. 23, where the values for both isentropic flat plates also appear.

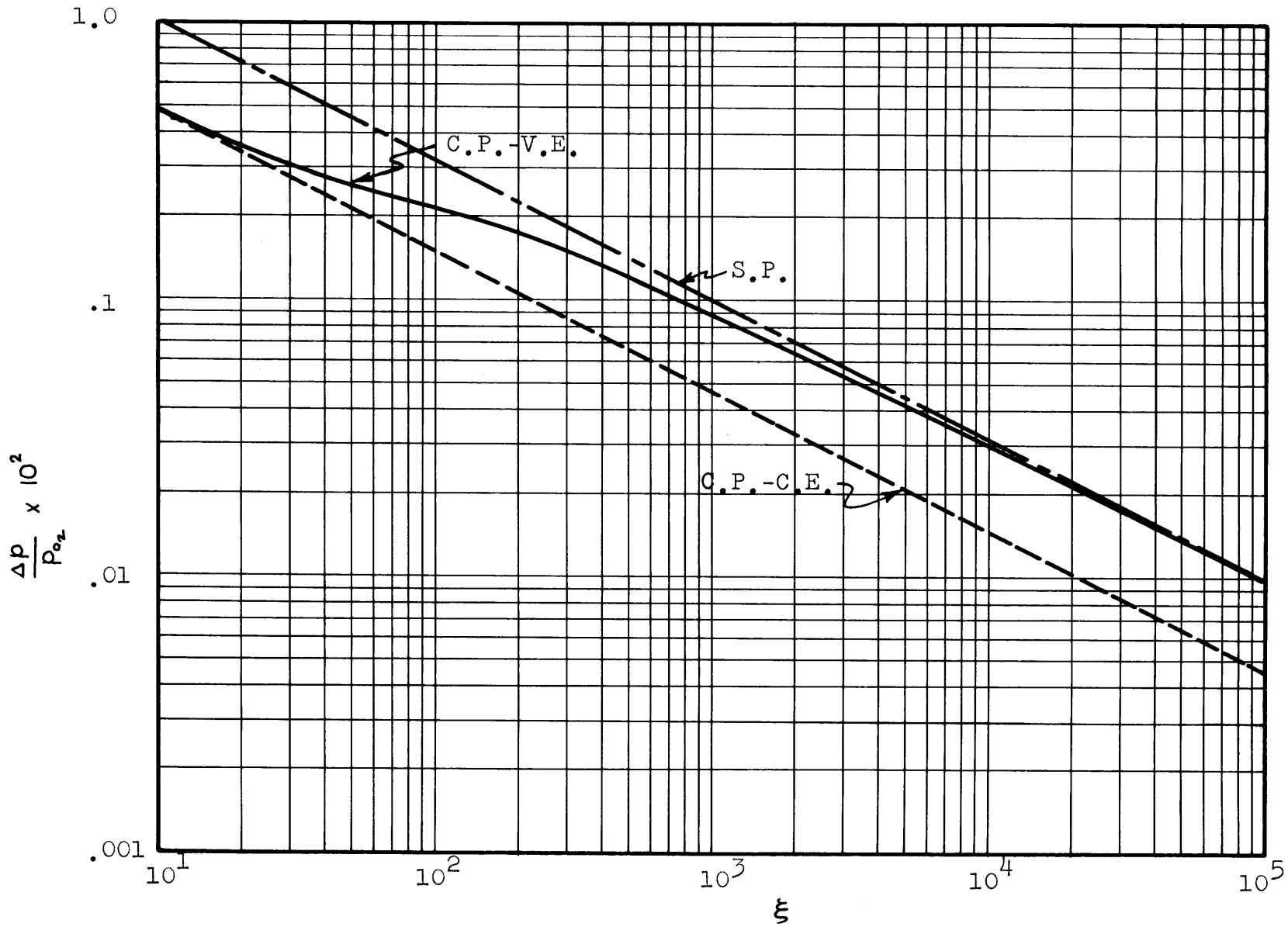

Figure 23 Boundary Layer Pressure Influence

CHAPTER 5

VARIABLE PRESSURE-VARIABLE ENTROPY CASE

5.1 The simplified non-isentropic solution derived in Chapter 4 included the assumption of constant static pressure. This is an approximation to the real case, where both the static and stagnation pressures vary along the plate. The solution of this more complex problem requires the use of the complete equations (3.17) and (3.18), which are rewritten below:

$$-\frac{d}{dx}\left[\rho_e U_e^2 \theta_s\right] + \rho_e U_e \theta_s \frac{dU_e}{dx} K_s +$$

$$+ \frac{dp_e}{dx}\left[\delta_s + \frac{\gamma-1}{2} M_e^2 (\theta_s + \delta_s^*)\right] = -\mu_{o_2} \frac{T_e}{T_{o_2}} \frac{U_e}{\theta_s} l_s \qquad (5.1)$$

and

$$\frac{dp_e}{dx} = \mu_{o_2}\left(\frac{T_e}{T_{o_2}}\right)^2 \frac{U_e}{\theta_s^2} m_s \qquad (5.2)$$

Equation (5.2) implies a dependence of the parameter m_s upon edge static pressure, temperature and velocity. Entropy gradients are assumed not to affect the static pressure distribution, but T_e and U_e <u>will</u> be affected by the entropy gradient. A variable m_s will, of course, imply variable l_s,

H_s, and K_s , which was not the case in the constant static pressure solution. The static pressure distribution remains as given in Chapter 2.

5.2 Derivation of the Momentum Equation

As in the constant static pressure case, the momentum equation (5.1) will be written in terms of the shock height $y_1(\xi)$ at which streamlines intersecting the boundary layer at $\delta(\xi)$ intersect the shock (see Fig. 17).

Equation (5.1) may be written as

$$-2U_e\Theta_s\frac{d}{dx}(\rho_e U_e\Theta_s)+2\Theta_s^2(K_s-1)\left[\rho_e U_e\frac{dU_e}{dx}+\frac{dp_e}{dx}\right]+$$

$$+2\frac{dp_e}{dx}\Theta_s^2\frac{T_{o_2}}{T_e}(H_s+1)=-2\mu_{o_2}\frac{T_e}{T_{o_2}}U_e l_s$$

Then, introducing the boundary condition (5.2) and collecting terms,

$$2U_e\Theta_s\frac{d}{dx}(\rho_e U_e\Theta_s)+2\Theta_s^2(1-K_s)\left[\rho_e U_e\frac{dU_e}{dx}+\frac{dp_e}{dx}\right]=$$

$$=2\mu_{o_2}\frac{T_e}{T_{o_2}}U_e\left[l_s+(H_s+1)m_s\right] \qquad (5.3)$$

The term $(1-K_s)$ and the brackets on the right-hand side of (5.3) may be written solely in terms of m_s as follows:

$$l_s+(H_s+1)m_s=\frac{1}{2}L_s-m_s$$

where L_s is the Thwaites parameter

$$L_s = 2\left[l_s + (H_s + 2)\, m_s\right] = .45 + 6 m_s ,$$

assuming Thwaites' linear universal relationship. Therefore,

$$l_s + (H_s + 1) m_s = \frac{1}{2}\left[.45 + 4 m_s\right]$$

With the universal relationship between K_s and m_s found in Chapter 3,

$$1 - K_s = 1.6 m_s - 5.2$$

If terms containing m_s in Eq. (5.3) are grouped together and the boundary condition (5.2) is used to substitute for m_s, the result is

$$2 U_e \theta_s \frac{d}{dx}\left(\rho_e U_e \theta_s\right) + \frac{3.2}{\mu_{o_2}}\left(\frac{T_{o_2}}{T_e}\right)^2 \frac{1}{U_e}\theta_s^4 \frac{dp_e}{dx}\left[\rho_e U_e \frac{dU_e}{dx} + \right.$$

$$\left. + \frac{dp_e}{dx}\right] - \theta_s^2\left[10.4\left(\rho_e U_e \frac{dU_e}{dx} + \frac{dp_e}{dx}\right) + 4\frac{T_{o_2}}{T_e}\frac{dp_e}{dx}\right] = \tag{5.4}$$

$$= .45\, \mu_{o_2} \frac{T_e}{T_{o_2}} U_e$$

Equation (5.4) illustrates the difficulty inherent in the variable pressure-variable entropy problem. The second

term on the left of (5.4) is non-linear. It will drop out for the isentropic case when

$$\frac{dp_e}{dx} = -\rho_e U_e \frac{dU_e}{dx} ,$$

and it will also vanish for the constant static pressure case when

$$\frac{dp_e}{dx} = 0$$

Essentially, then, the mathematical simplification introduced in the solutions previously found was a linearization of the momentum equation.

The shock intersection height y_1 will now be introduced by again using the shock-boundary layer mass balance equation.

$$\rho_e U_e \theta_s = \rho_1 U_1 \frac{y_1}{K_s} \qquad (5.5)$$

Again, it must be noted that in (5.5), K_s will be a variable for the variable pressure case.

Substituting for $\rho_e U_e \theta_s$ in (5.4) from (5.5), and non-dimensionalizing the result, (5.4) becomes

$$\frac{d\zeta}{d\xi} + \frac{3.2D}{\mu_{O_2}} \left(\frac{T_{O_2}}{T_e}\right)^2 \frac{\rho_e}{U_e} \frac{(\rho_1 U_1)^2}{(\rho_e U_e)^4} \zeta^2 \left\{ \frac{dp_e}{d\xi} \left[\rho_e U_e \frac{dU_e}{d\xi} + \right.\right.$$

$$\left.\left. + \frac{dp_e}{d\xi} \right]\right\} - \zeta \left[10.4 \frac{1}{U_e} \frac{dU_e}{d\xi} + \frac{4}{\rho_e U_e^2} \frac{dp_e}{d\xi} \left(2.6 + \frac{T_{O_2}}{T_e} \right) \right] =$$

$$= \frac{.45 \mu_{O_2}}{D} \frac{T_e}{T_{O_2}} \frac{\rho_e U_e}{(\rho_1 U_1)^2} \tag{5.6}$$

where $$\zeta = \left(\frac{Y_1}{K_s D}\right)^2$$

and $$\xi = \frac{x}{D}$$

Equation (5.6) is of the general form

$$\frac{d\zeta}{d\xi} + P(\xi)\zeta^2 - Q(\xi)\zeta = R(\xi) \tag{5.7}$$

The coefficients in (5.6) have been rewritten in terms of Mach number and temperature and pressure ratios to simplify calculations. The results are

$$P(\xi) = \frac{J}{M_e^4} \left(\frac{p_{O_2}}{p_e}\right)^2 \left(\frac{T_{O_2}}{T_e}\right)^{3/2} \frac{d(p_e/p_{O_2})}{d\xi} \left[\frac{T_e}{T_{O_2}} \frac{dM_e}{d\xi} + \right.$$

$$\left. + \frac{1}{\gamma M_e} \frac{p_{O_2}}{p_e} \frac{d(p_e/p_{O_2})}{d\xi} \right] \tag{5.8a}$$

where

$$J = \frac{3.2}{\gamma} Re_{D_2} \frac{T_{o_1}}{T_1} \left(\frac{p_1}{p_{o_2}}\right)^2 M_1^2 = 302.26$$

$$Q(\xi) = \frac{1}{M_e}\left[10.4 \frac{T_e}{T_{o_2}} \frac{dM_e}{d\xi} + \right.$$

$$\left. + \frac{4}{\gamma M_e} \frac{p_{o_2}}{p_e} \frac{d(p_e/p_{o_2})}{d\xi}\left(2.6 + \frac{T_{o_2}}{T_e}\right)\right] \qquad (5.8b)$$

$$R(\xi) = G \frac{p_e}{p_{o_2}}\left[\frac{T_e}{T_{o_2}} M_e^2\right]^{1/2} \qquad (5.8c)$$

where

$$G = \frac{.45}{Re_{D_2} M_1^2}\left(\frac{p_{o_2}}{p_1}\right)^2 \frac{T_1}{T_{o_2}} = 3.137 \times 10^{-3}$$

The boundary condition (5.2), after introducing (5.5) and non-dimensionalizing, becomes

$$m_s = J' \frac{1}{M_e^3}\left(\frac{T_{o_2}}{T_e}\right)^{3/2}\left(\frac{p_{o_2}}{p_e}\right)^2 \zeta \frac{d(p_e/p_{o_2})}{d\xi} \qquad (5.9)$$

where

$$J' = \frac{Re_{D_2}}{\gamma} \frac{T_{o_1}}{T_1}\left(\frac{p_1}{p_{o_2}}\right)^2 M_1^2 = \frac{J}{3.2}$$

5.3 Solution of the Momentum Equation

It has been argued previously that near the leading edge of the plate the flow will be isentropic, and that for downstream the static pressure will be constant. It will be useful to determine the range over which these assumptions can be made, because in both cases the momentum equation becomes linear and the solutions found in Chapters 2 and 4 will apply. The intermediate region will have to be treated by the complete non-linear equation (5.7), but the effort required to obtain a solution will be reduced by applying (5.7) to only this intermediate range, rather than the complete range of ξ . For purposes of determining the extent of this intermediate region, Figure 24 has been plotted. It shows the edge Mach number distributions for the variable pressure-constant entropy case treated in Chapter 2, and for the constant pressure-variable entropy case treated in Chapter 4. For $0 < \xi < 6$, Fig. 24 shows that non-isentropic effects are unimportant, because the assumed edge Mach number in the constant pressure-variable entropy solution has remained constant. For $200 < \xi < +\infty$, Fig. 24 shows that variable pressure effects are not important, because the isentropic Mach number distribution is constant, indicating that the static pressure is constant. Non-linear effects must therefore be considered in the range $6 < \xi < 200$

Due to the non-linear nature of Eq. (5.7), the problem requires a numerical solution. In addition, an iterative

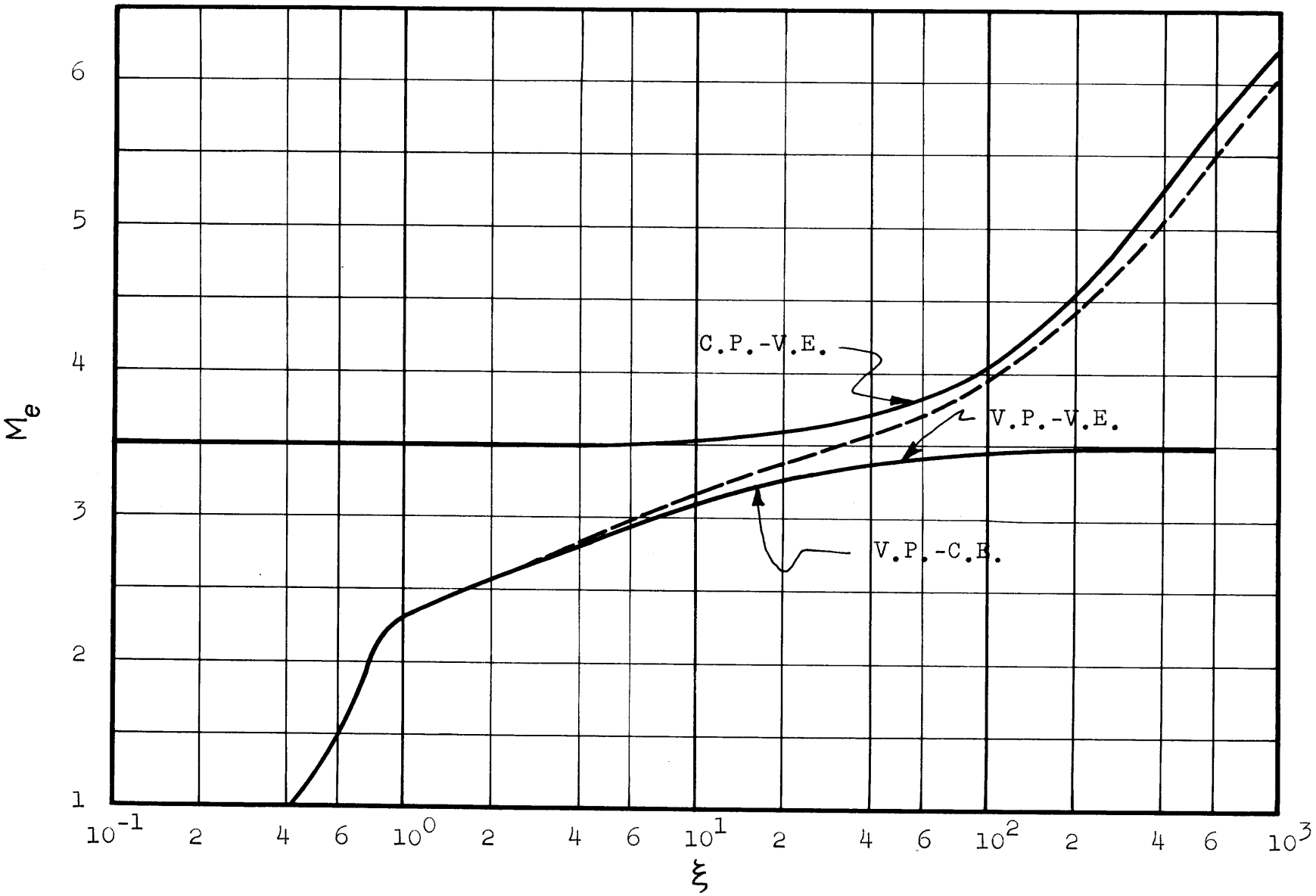

Figure 24 Edge Mach Number Distributions for Isentropic and Non-Isentropic Cases

scheme analogous to that used in Chapter 4 must be devised. The procedure may go as follows:

1. Assume an edge Mach number distribution over the range $6 < \xi < 200$.

2. With coefficients obtained from this edge Mach number distribution, solve Eq. (5.7) for ζ by some numerical scheme.

3. Use the boundary condition (5.9) to obtain m_s .

4. Obtain K_s from m_s by the universal relationship

$$K_s = -1.6 m_s + 6.2$$

found in Chapter 3.

5. With K_s and ζ obtain

$$\eta = \left(\frac{Y_1}{D}\right)^2 = \zeta K_s^2$$

6. With this distribution of η obtain the shock inlination angle at the intersection point Y_1 from the relationship

$$\phi = \tan^{-1}\left[.1328\sqrt{\frac{57.845}{\eta} + 1}\right]$$

derived in Chapter 3 from Love's approximate shock shape.

7. With the local shock inclination angle ϕ obtain the stagnation pressure immediately behind the shock, which is the same as the stagnation pressure p_{o_e} at the edge of the boundary layer.

8. With this value of the stagnation pressure calculate the ratio

$$\frac{p_e}{p_{o_e}} = \frac{p_e}{p_{o_2}} \cdot \frac{p_{o_2}}{p_{o_e}}$$

from which a new edge Mach number distribution may be obtained by using isentropic relationships.

9. Continue the iterative scheme until two consecutive edge Mach number distributions lie as closely as desired.

5.4 Calculation of Edge Mach Number Distribution

The numerical scheme described above was programmed for the IBM 709 computer of the MIT Computation Center. The range considered was $.8 \leq \xi \leq 1000$ to insure that the variable pressure-variable entropy solution would fair into the variable pressure-constant entropy and constant pressure-variable entropy solutions, as expected. The program devised is described in Appendix B. Only details concerning inputs and the criterion for convergence are given here.

In order to calculate the coefficients $P(\xi)$, $Q(\xi)$ and $R(\xi)$ of Eq. (5.7), it is necessary to start out with an edge Mach number $M_e(\xi)$, a slope of the edge Mach number $(dM_e/d\xi)$, a pressure ratio (p_e/p_{o_2}), and a slope of this pressure ratio $[d(p_e/p_{o_2})/d\xi]$. The initial guess at the Mach number distribution was obtained by fairing in a smooth curve between the V.P.-C.E. and C.P.-V.E. curves of Fig. 24, and then simply reading input values of M_e off

this curve. $(dM_e/d\xi)$ was obtained by a numerical scheme which gave this quantity as a function of the value of M_e at different points (see Appendix B). Since all the points considered were downstream of the shoulder, Love's pressure formula (Eq. (2.1)) was used to obtain (p_e/p_{o_2}). This equation was differentiated to obtain $d(p_e/p_{o_2})/d\xi$. The result is

$$\frac{d(p_e/p_{o_2})}{d\xi} = \frac{2}{3}\frac{p_3}{p_{o_2}}\left\{\frac{1}{(\xi-\xi_s)^{5/3}\left[1+(\xi-\xi_s)^{-\frac{2}{3}}\right]\left(\frac{p_3}{p_1}+1\right)} - \frac{1}{\left[1+(\xi-\xi_s)^{2/3}\right]^2(\xi-\xi_s)^{1/3}}\right\} \tag{5.10}$$

It should be noted that this equation becomes singular at $\xi = \xi_s$, but since this point was not included in the calculations this singularity is of no concern here.

Calculations were stopped when all consecutive values of M_e at corresponding values of ξ were found to be within .005 of each other.

The results of these calculations are plotted in Fig. 24 - indicated by the dotted curve labeled (V.P.-V.E.). It is evident that at high values of ξ this curve does not merge with the C.P.-V.E. solution, as it should. This arises from an inconsistency in the choice of the numerical value of the parameter $K_s(m_s) = \frac{\delta - \delta^*}{\theta}$

For the variable pressure case, this parameter is given by the universal relationship found in Chapter 3.

$$K_s = -1.6\, m_s + 6.2$$

This equation will yield a value

$$K_s(0) = 6.2$$

for $m_s = 0$ ($d(p_e/p_{o_2})/d\xi = 0$). For the constant pressure case K_s was a constant everywhere and was found to have a numerical value of 6.43, from the Blasius solution. The smaller K_s in the variable pressure-variable entropy solution will give a smaller η since

$$\eta = \xi K_s^2$$

This smaller η will give a larger local shock angle ϕ, since η enters into the expression for ϕ as $\sqrt{1/\eta}$ (see Eq. (3.28)). This greater ϕ will give a smaller value of M_e. The difference between the dotted and solid curves of Fig. 24 is, however, quite small (of the order of 4%). At low values of ξ the V.P.-V.E. curve does fair smoothly into the V.P.-C.E. solution.

5.5 Calculation of Boundary Layer Properties and Pressure Influence

5.5.1 Momentum Thickness

The momentum thickness may again be obtained from the

shock-boundary layer mass balance condition (4.7), as was done in Chapter 4. The result is

$$\frac{\theta}{D} = \frac{C'}{M_e} \frac{p_{o_2}}{p_e} \sqrt{\frac{T_e}{T_{o_2}} \zeta} \tag{5.11}$$

where

$$C' = \frac{p_1}{p_{o_2}} M_1 \sqrt{\frac{T_{o_1}}{T_1}} = .3597 \tag{5.11a}$$

With the Mach number distribution shown in Fig. 24, this equation has been plotted in Fig. 25, where the momentum thickness for the V.P.-C.E. and C.P.-V.E. cases also appears.

5.5.2 Displacement Thickness

The displacement thickness may be obtained from

$$\frac{\delta^*}{D} = H \frac{\theta}{D} \tag{5.12}$$

where

$$H = \frac{T_{o_2}}{T_e}(H_s + 1) - 1 = H_s + \frac{\gamma - 1}{2} M_e^2 (H_s + 1) \tag{5.12a}$$

as given by the Howarth transformation (see Section 4.3.3). As previously stated, H_s corresponds to the ratio of an incompressible displacement thickness to an incompressible momentum thickness, and with the values of m_s found in the calculation of $M_e(\xi)$, it may be obtained from Thwaites[5]

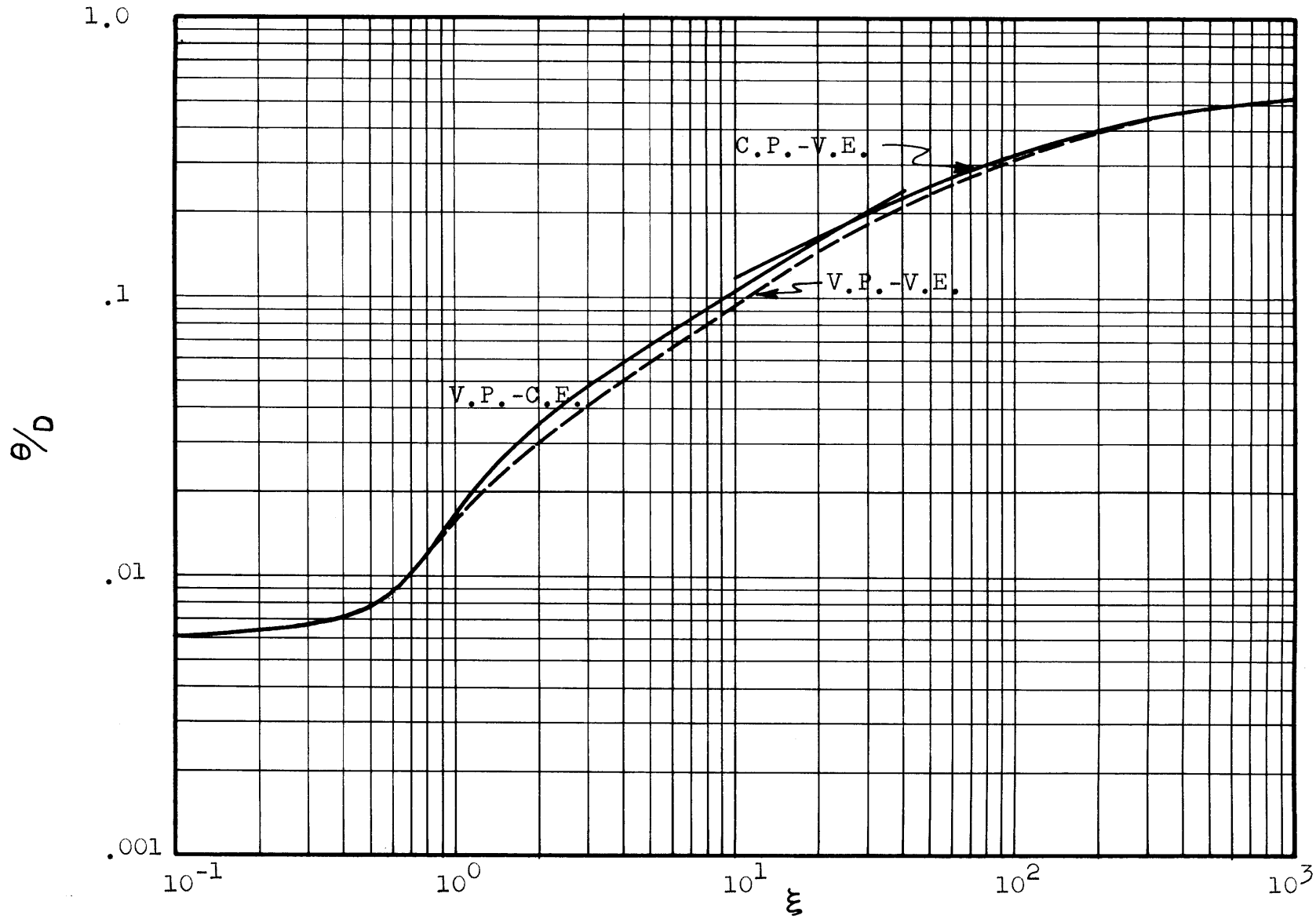

Figure 25 Momentum Thickness Distribution for V.P.-V.E. Case

Table I. This non-dimensional displacement thickness is plotted in Fig. 26, where the V.P.-C.E. and C.P.-V.E. cases also appear.

5.5.3 Pressure Influence

In order to obtain the contribution of the boundary layer to the pressure distribution along the plate, it is necessary to calculate the displacement thickness slope $\left[d(\delta^*/D)/d\xi \right]$. From Equation (5.12)

$$\frac{d(\delta^*/D)}{d\xi} = H \frac{d(\theta/D)}{d\xi} + \frac{\theta}{D} \frac{dH}{d\xi} \tag{5.13}$$

With Equation (5.11) and the non-linear momentum equation (5.7),

$$\frac{d(\theta/D)}{d\xi} = \frac{C'}{M_e} \frac{p_{o_2}}{p_e} \sqrt{\frac{T_e}{T_{o_2}} \zeta} \left\{ \frac{1}{2\zeta} \left[R + \zeta \left(Q - .4 \frac{T_e}{T_{o_2}} M_e \frac{dM_e}{d\xi} \right) - \right. \right. \tag{5.14}$$

$$\left. \left. - P\zeta^2 \right] - \frac{1}{M_e} \frac{dM_e}{d\xi} - \frac{p_{o_2}}{p_e} \frac{d(p_e/p_{o_2})}{d\xi} \right\}$$

where P, Q, and R are given by Eqs. (5.8a, b, c).

With the transformation for H (5.12a),

$$\frac{dH}{d\xi} = \frac{dH_s}{d\xi} \frac{T_{o_2}}{T_e} + (\gamma - 1)(H_s + 1) M_e \frac{dM_e}{d\xi} \tag{5.15}$$

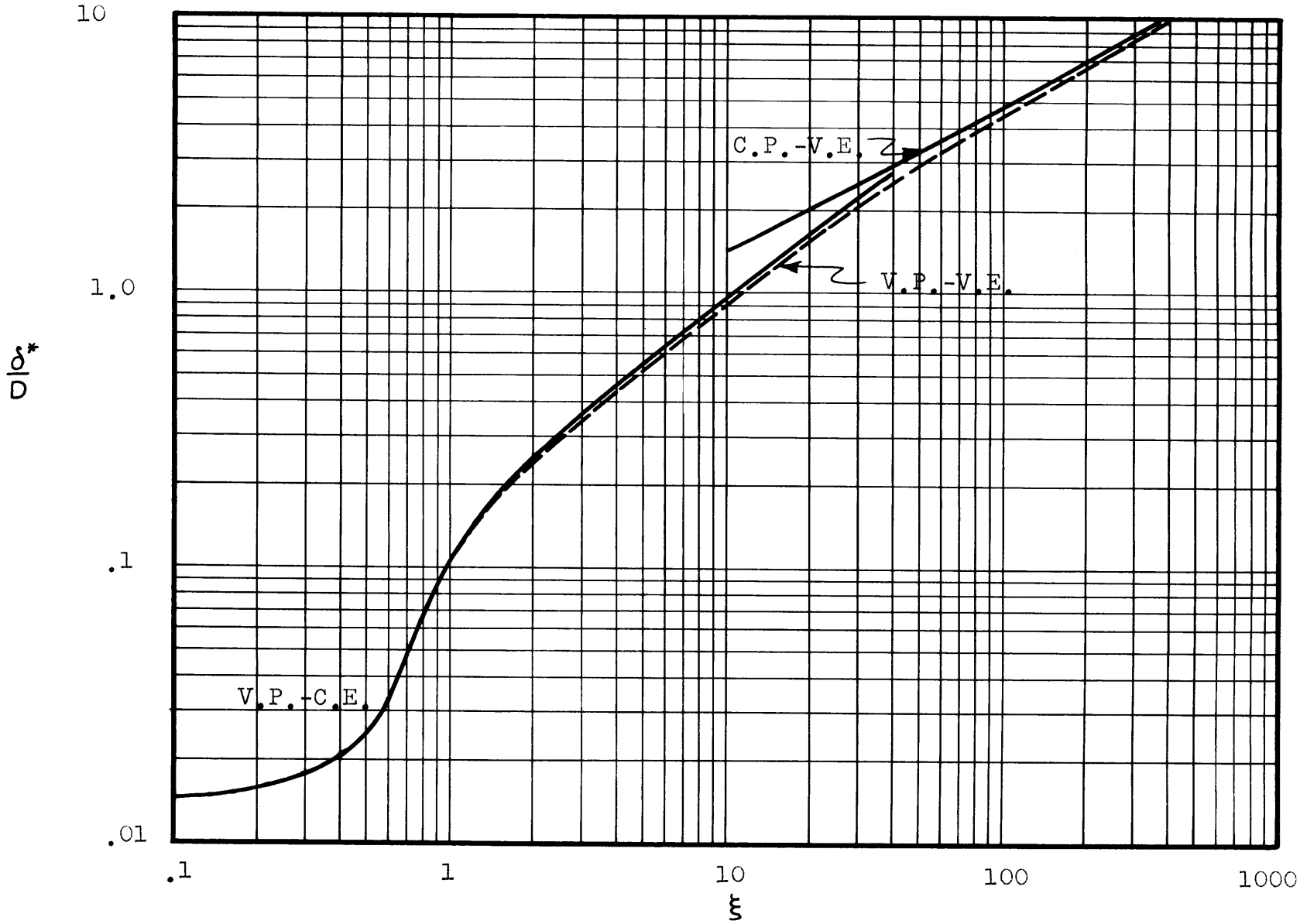

Figure 26 Displacement Thickness Distribution for V.P.-V.E. Case

Equations (5.13), (5.14) and (5.15) will then yield the displacement thickness slope which may then be used for calculating the boundary layer contribution to the pressure distribution through the Prandtl-Meyer relationship

$$\frac{\Delta p}{p_{o_2}} = \frac{\gamma M_e^2}{(M_e^2-1)^{1/2}} \frac{p_e}{p_{o_2}} \frac{d(\delta^*/D)}{d\xi} \tag{5.16}$$

This last expression has been plotted in Fig. 27, where the V.P.-C.E. and C.P.-V.E. cases also appear.

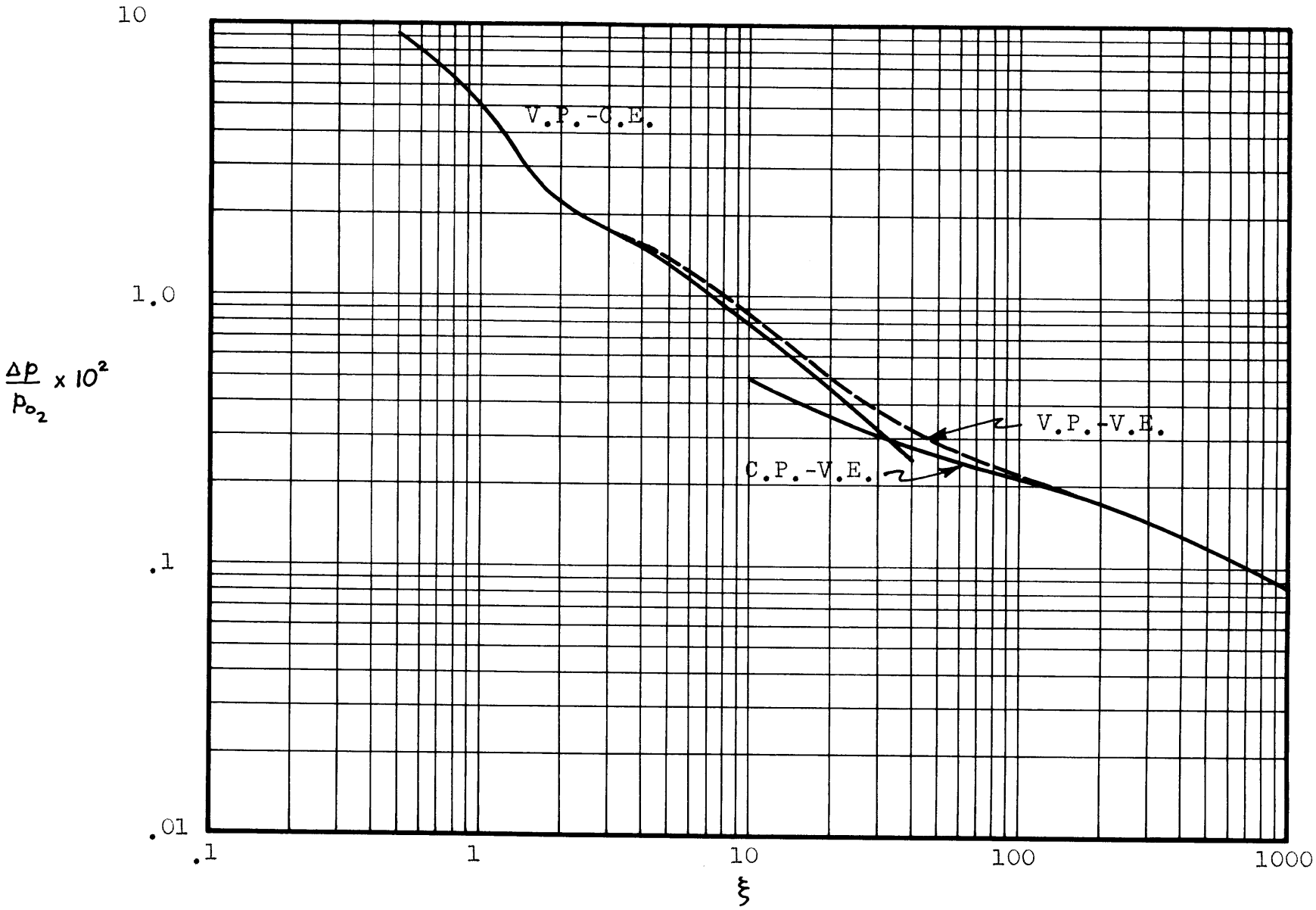

Figure 27 Boundary Layer Pressure Influence for V.P.-V.E. Case

CHAPTER 6

CONCLUSIONS AND SUGGESTIONS FOR FURTHER WORK

6.1 Restatement of Problem Solved and Outline of Solutions

The object of this paper has been to calculate the contribution of the boundary layer to the surface pressure distribution along a blunt flat plate of large length-to-thickness ratio submerged in a hypersonic stream. Account was taken of variable stagnation conditions at the edge of the boundary layer produced by the curved bow shock.

The problem was approached by integral methods coupled with Thwaites' approximate relationships between first and second derivatives of the velocity at the surface. The flow was at first assumed to be isentropic to provide limits which non-isentropic results should approach near the leading edge and far from the leading edge. The isentropic assumption was then removed and the stagnation pressure allowed to vary along the edge of the boundary layer. As a simplifying assumption, however, the static pressure was considered to be constant along the plate. Finally the complete problem with variable static and stagnation pressures was solved. This last solution was seen to fair smoothly into the variable pressure-constant entropy solution near the leading edge and to be

very close to the constant pressure-variable entropy solution far downstream. The reason for the small discrepancy found in the latter asymptote is explained in Chapter 5.

6.2 Effects of the Entropy Gradient

The entropy gradient produced by the curved bow shock reduces the momentum thickness below its isentropic value (see Fig. 20). Figure 21 shows that the displacement thickness is increased by a small amount by the entropy gradient. The pressure disturbance produced by the boundary layer is seen to be small everywhere, and to be increased by the entropy gradient (Fig. 23). All of these quantities approach the correct asymptotes near the leading edge and far downstream. This behavior has been discussed and explained in previous chapters.

This paper has shown that the presence of the boundary layer will only modify inviscid results by a maximum of about 10% at the leading edge (see Fig. 12). It should be pointed out, however, that as the free stream Mach number is increased, driving the shock closer to the surface, and as the Reynolds number is decreased, making the boundary layer thicker, the boundary layer should contribute a greater percentage of the surface pressure. For long plates, the entropy gradient

produced by the curved bow shock tends to increase the contribution of the boundary layer to the pressure distribution.

6.3 Suggestions for Further Work

The results presented in this paper should be confirmed experimentally and extended theoretically.

Experimentally, it would be interesting to obtain boundary layer profiles for plates of large length-to-thickness ratio. The large length-to-thickness ratio at which non-isentropic effects become important will make impractical the testing of plates at the free stream Mach and Reynolds numbers considered here. However, an increase of Mach number and a reduction of Reynolds number may be expected to increase the importance of non-isentropic effects as well as reduce the length-to-thickness ratio at which they become significant. The most practical of these possibilities is perhaps the reduction of the Reynolds number. Since the boundary layer will then be thicker, it will be "swallowed" into the variable entropy region sooner, and the interesting length-to-thickness ratio will thus be reduced. It should be noted that the Reynolds number should not be reduced too much, because if this is done, difficulties will arise for the following cases:

1. The boundary layer near the nose may no longer be distinct from the shock layer.

2. The inviscid velocity gradient at the edge of the boundary layer may become significant, thus eliminating the possibility of considering non-isentropic effects to affect only the stagnation pressure at the edge of the boundary layer.

The theoretical predictions presented here should be extended to other free stream Mach and Reynolds numbers, mainly to determine the range of these parameters at which experimental studies could be conducted. Furthermore, it would be interesting to remove the assumption of zero heat transfer at the surface and obtain an indication of how shock-induced entropy gradients affect the heat transfer at the surface. The study of non-isentropic effects in the axisymmetric case will also be of interest, since axisymmetric bodies of large length-to-thickness ratio are often encountered in practice. The body of a blunt missile traveling at high speeds would provide such an example.

APPENDIX A

DERIVATION OF THE BOUNDARY LAYER MOMENTUM INTEGRAL

The boundary layer equations are:

Continuity $$\frac{\partial(\rho u)}{\partial x} + \frac{\partial(\rho v)}{\partial y} = 0 \qquad (A.1)$$

Momentum $$\rho\left[u\frac{\partial u}{\partial x} + v\frac{\partial u}{\partial y}\right] = -\frac{dp_e}{dx} + \frac{\partial}{\partial y}\left(\mu\frac{\partial u}{\partial y}\right) \qquad (A.2)$$

Integrating (A.2) with respect to y from o to δ :

$$\int_0^\delta \rho u\frac{\partial u}{\partial x}\,dy + \int_0^\delta \rho v\frac{\partial u}{\partial y}\,dy = -\int_0^\delta \frac{dp_e}{dx}\,dy + \mu_w\left(\frac{\partial u}{\partial y}\right)_{y=0} \qquad (A.3)$$

The second term on the left-hand side of (A.3) may be integrated by parts to give

$$\int_0^\delta \rho v\frac{\partial u}{\partial y}\,dy = \rho_e V_e U_e - \int_0^\delta u\frac{\partial(\rho v)}{\partial y}\,dy$$

Then from the continuity equation (A.1),

$$\rho_e V_e = -\int_0^\delta \frac{\partial(\rho u)}{\partial x}\,dy$$

Equation (A.3) therefore becomes

$$\int_0^\delta \rho u \frac{\partial u}{\partial x} dy - U_e \int_0^\delta \frac{\partial(\rho u)}{\partial x} dy + \int_0^\delta u \frac{\partial(\rho u)}{\partial x} dy =$$

$$= - \int_0^\delta \frac{dp_e}{dx} dy - \mu_w \left(\frac{\partial u}{\partial y}\right)_{y=0} \qquad (A.4)$$

If, as customary, the static pressure is assumed constant across the boundary layer, and account is taken of the fact that from the energy equation $T_w = T_{o_2}$, and therefore $\mu_w = \mu_{o_2}$, then after collecting terms, (A.4) becomes

$$\int_0^\delta \rho u \frac{\partial u}{\partial x} dy + \int_0^\delta \frac{\partial(\rho u)}{\partial x} (u - U_e) dy = - \frac{dp_e}{dx} \delta - \mu_{o_2} \left(\frac{\partial u}{\partial y}\right)_{y=0}$$

This may be written as

$$\frac{d}{dx} \int_0^\delta \rho u (u - U_e) dy + \frac{dU_e}{dx} \int_0^\delta \rho u \, dy + \frac{dp_e}{dx} \delta = - \mu_{o_2} \left(\frac{\partial u}{\partial y}\right)_{y=0}$$

or

$$- \frac{d}{dx} \left[\rho_e U_e^2 \int_0^\delta \frac{\rho u}{\rho_e U_e} \left(1 - \frac{u}{U_e}\right) dy \right] + \rho_e U_e \frac{dU_e}{dx} \int_0^\delta \frac{\rho u}{\rho_e U_e} dy +$$

$$+ \frac{dp_e}{dx} \delta = - \mu_{o_2} \left(\frac{\partial u}{\partial y}\right)_{y=0} \qquad (A.5)$$

Now

$$\int_0^{\delta} \frac{\rho u}{\rho_e U_e}\left(1 - \frac{u}{U_e}\right) dy \equiv \theta$$

and

$$\delta^* = \int_0^{\delta}\left(1 - \frac{\rho u}{\rho_e U_e}\right) dy = \delta - \int_0^{\delta} \frac{\rho u}{\rho_e U_e}\, dy,$$

or

$$(\delta - \delta^*) = \int_0^{\delta} \frac{\rho u}{\rho_e U_e}\, dy$$

Equation (A.5) may then be written as

$$-\frac{d}{dx}\left[\rho_e U_e \theta\right] + \rho_e U_e (\delta - \delta^*)\frac{dU_e}{dx} + \frac{dp_e}{dx}\delta = = -\mu_{o_2}\left(\frac{\partial u}{\partial y}\right)_{y=0} \qquad \text{(A.6)}$$

This last equation is the same as Eq. (3.6) in the text.

APPENDIX B

COMPUTER PROGRAM

B.1 The computations required in the variable pressure-variable entropy solution described in Chapter 5 were performed by the IBM 709 computer of the MIT Computation Center. A brief outline of the salient features of the program is given in this section. As described in the text, the inputs were an assumed Mach number distribution $[M_e(\xi)]$, and a pressure distribution $[p_e/p_{o_2}(\xi)]$. Figure B.1 is a simplified flow chart of the program. Two steps in the procedure are worthy of further note. The first of these is the calculation of the coefficients $P(\xi)$, $Q(\xi)$ and $R(\xi)$ which enter into the non-linear differential equation (5.7). The second is the numerical solution of this non-linear equation to obtain ζ.

B.2 Calculation of Coefficients

The expressions for $P(\xi)$ and $Q(\xi)$ given by Eqs. (5.8a) and (5.8b) involve the derivatives $\left[d(p_e/p_{o_2})/d\xi\right]$ and $dM_e/d\xi$. $d(p_e/p_{o_2})/d\xi$ was obtained by differentiating

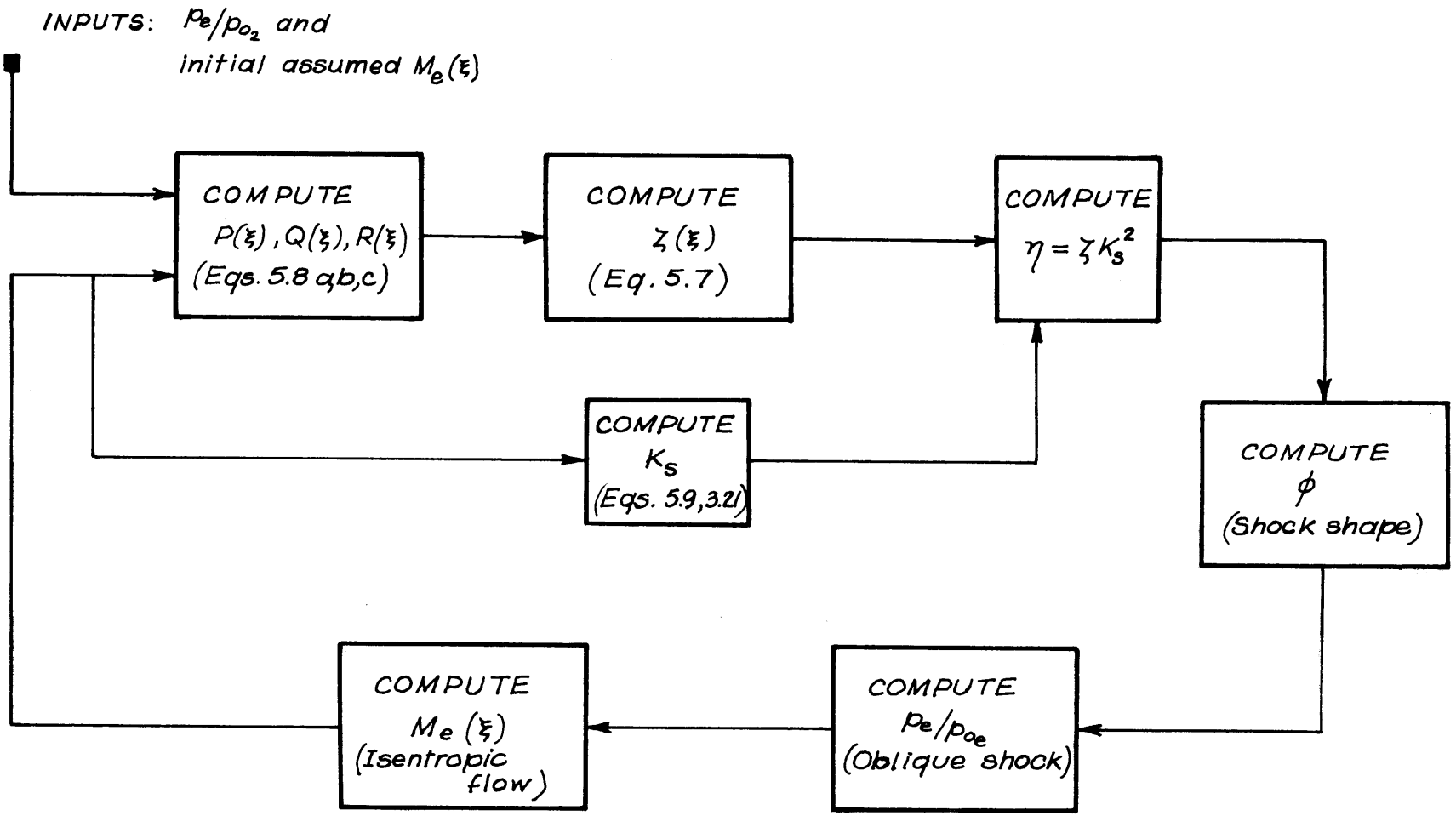

Figure B.1 Computer Program Flow Chart

Calculations were performed at ξ = .8, 2, 4, 6, 10, 20, 40, 60, 100, 200, 400, 600, 1000

Love's[1] pressure formula, as described in the text. There is, however, no analytic expression describing the first assumed Mach number distribution. It was therefore necessary to obtain $dM_e/d\xi$ by a numerical scheme which consists of differentiating Lagrange's interpolation formula for uneven intervals of the independent variable (Ref. 13). Lagrange's polynomial matches a given set of points exactly at the interval desired, and approximates the function between these points by a polynomial. For this particular calculation, four points were taken at which the function was forced to have the correct value. Between these points $M_e(\xi)$ was approximated by a third order polynomial. Figure B.2 illustrates this approach for an arbitrary function $y(x)$.

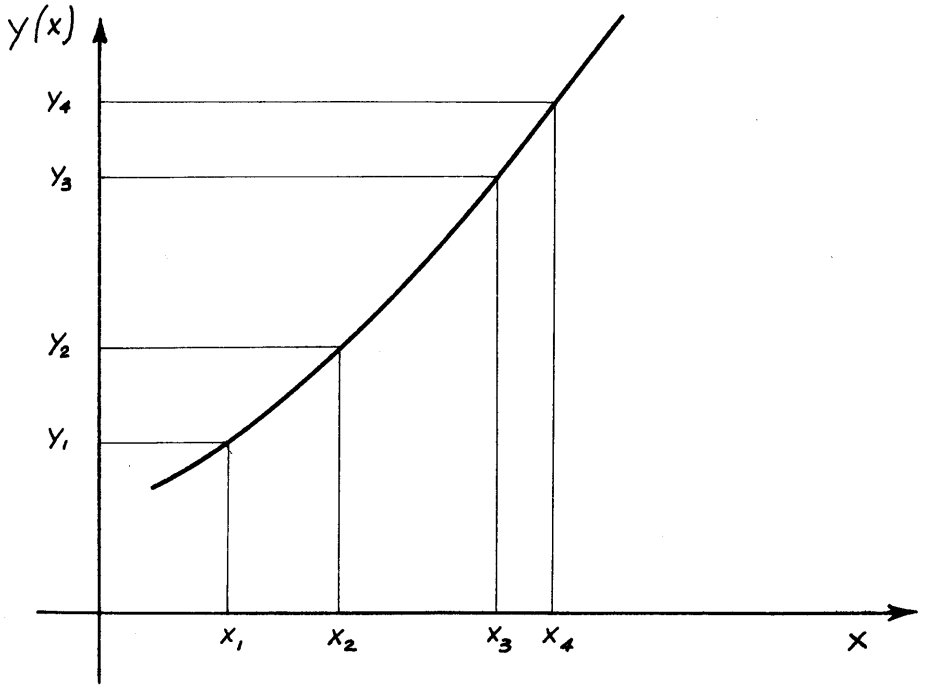

Figure B.2

Lagrange's polynomial approximation is written then as

$$y(x) \approx \frac{(x-x_2)(x-x_3)(x-x_4)}{(x_1-x_2)(x_1-x_3)(x_1-x_4)}\, y_1 + \frac{(x-x_1)(x-x_3)(x-x_4)}{(x_2-x_1)(x_2-x_3)(x_2-x_4)}\, y_2 +$$

$$+ \ldots\ldots\ldots\ldots = \sum_{m=1}^{4} \frac{y_m}{\prod_{\substack{n=1 \\ n\neq m}}^{4} (x_m - x_n)} \cdot \frac{\prod_{n=1}^{4} (x-x_n)}{(x-x_m)} \qquad \text{(B.1)}$$

Equation (b.1) gives the correct values of $y(x)$ at $x = x_i$ $(i = 1, 4)$, and spans the space between these points by a sum of third-order polynomials.

Differentiating (B.1), the slope is given by

$$\frac{dy}{dx} = \sum_{m=1}^{4} \frac{y_m}{\prod_{\substack{n=1 \\ n\neq m}}^{4} (x_m - x_n)} \frac{d}{dx}\left[\frac{\prod_{n=1}^{4} (x-x_n)}{(x-x_m}\right]$$

or

$$\frac{dy}{dx} = \sum_{m=1}^{4} \frac{y_m}{\prod_{\substack{n=1 \\ n\neq m}}^{4} (x_m - x_n)} \left\{ \frac{\frac{d}{dx}\left[\prod_{n=1}^{4} (x-x_n)\right]}{(x-x_m)} - \frac{\prod_{n=1}^{4} (x-x_n)}{(x-x_n)^2} \right\} \qquad \text{(B.2)}$$

Now $$\frac{d}{dx}\left[\prod_{n=1}^{4} (x-x_n)\right] = \sum_{k=1}^{4} \prod_{\substack{n=1 \\ n\neq k}}^{4} (x-x_n)$$

and (B.2) then becomes

$$\frac{dy}{dx} \approx \sum_{m=1}^{4} \frac{y_m}{\prod_{\substack{n=1 \\ n\neq m}}^{4} (x_m - x_n)} \left\{ \frac{\sum_{k=1}^{4} \prod_{\substack{n=1 \\ n\neq k}}^{4} (x - x_n)}{(x - x_m)} - \frac{\prod_{n=1}^{4} (x - x_n)}{(x - x_m)^2} \right\}$$

(B.3)

It is helpful to write out completely one of the terms in the braces of (B.3). For $m = 2$, for instance, this will be

$$\frac{(x-x_2)(x-x_3)(x-x_4)}{(x-x_2)} + \frac{(x-x_1)(x-x_3)(x-x_4)}{(x-x_2)} +$$

$$+ \frac{(x-x_1)(x-x_2)(x-x_4)}{(x-x_2)} + \frac{(x-x_1)(x-x_2)(x-x_3)}{(x-x_2)} -$$

$$- \frac{(x-x_1)(x-x_2)(x-x_3)(x-x_4)}{(x-x_2)^2} =$$

$$= (x-x_3)(x-x_4) + (x-x_1)(x-x_4) + (x-x_1)(x-x_3)$$

(B.4)

If the derivative <u>at the point x_1</u> is now desired (*i.e.*) $dy/dx\,(x_1)$, the only term surviving in (B.4) will be

$$(x_1 - x_3)(x_1 - x_4) \qquad \text{(B.5a)}$$

For $m = 3$, the only term left in the braces will be

$$(x_1 - x_2)(x_1 - x_4) \quad ; \tag{B.5b}$$

and for $m = 4$

$$(x_1 - x_2)(x_1 - x_3) \tag{B.5c}$$

It may also be verified that for $m = 1$, the brackets of (B.3) reduce to the sum of equations (B.5), i.e.,

$$(x_1 - x_3)(x_1 - x_4) + (x_1 - x_2)(x_1 - x_4) + (x_1 - x_2)(x_1 - x_3) \tag{B.6}$$

If these products are then arranged in a one-row matrix, this matrix will have the last three elements equal to all possible products of differences $(x_1 - x_i)$ where i is <u>not</u> equal to the row of the matrix and <u>not</u> equal to the column. The first element in this matrix will be equal to the sum of the last three elements. Such a matrix was set up by the computer program in order to calculate the derivative $dM_e/d\xi$ at $\xi_1 = .8$.

For calculating the derivative at other points ξ_i , $(i = 2,13)$ the procedure was repeated by shifting the range of four points down by one, so that the point at which the derivative was calculated was always the first of a set of 4. This procedure is illustrated in Fig. B.3.

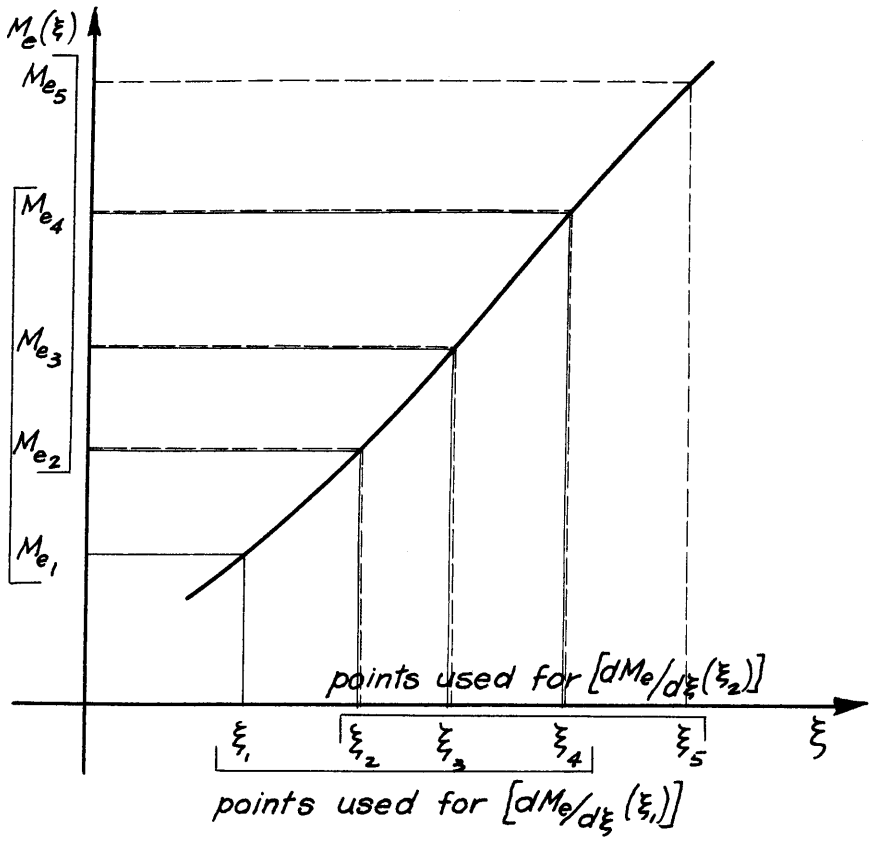

Figure B.3

In order to calculate $dM_e/d\xi$ at the thirteen points listed in Fig. B.1, it was therefore necessary to introduce seventeen values of ξ and seventeen corresponding values of $M_e(\xi)$.

B.3 Calculation of ζ

After the quantities P, Q and R have been obtained, it is necessary to calculate ζ from the ordinary non-linear first order differential equation

$$\frac{d\zeta}{d\xi} + P(\xi)\zeta^2 - Q(\xi)\zeta = R(\xi) \tag{B.7}$$

This was done by a numerical scheme described below.

For any arbitrary function $y(x)$, the following is true:

$$y_{n+1} = y_n + \int_{x_n}^{x_{n+1}} \frac{dy}{dx}\, dx \tag{B.8}$$

where

$$y_{n+1} = y(x_{n+1})$$
$$y_n = y(x_n)$$

In terms of (B.7), then

$$\zeta_{n+1} = \zeta_n + \int_{\xi_n}^{\xi_{n+1}} \frac{d\zeta}{d\xi}\, d\xi$$

or

$$\zeta_{n+1} = \zeta_n + \int_{\xi_n}^{\xi_{n+1}} \left[R + Q\zeta - P\zeta^2\right] d\xi \tag{B.9}$$

The question is how to approximate the integrand in (B.9) in order to calculate ζ_{n+1} when ζ_n is known. An iterative scheme was used. A first approximation $\zeta_{n+1}^{(1)}$

was calculated by using the value of the integrand at ξ_n . With this $\zeta^{(1)}_{n+1}$, an average value of the integrand was computed to obtain a $\zeta^{(2)}_{n+1}$. This value was then used to obtain a second average for the integrand. This iterative scheme was continued until two consecutive values of ζ_{n+1} were found to lie within .05% of each other. The first value of ζ (at $\xi_1 = .8$) was calculated from the isentropic solution (V.P.-C.E.).

REFERENCES

1. Love, "Prediction of Inviscid Induced Pressures from Round Leading Edge Blunting at Hypersonic Speeds," ARS Journal, October 1959.

2. Ferri, A., The Influence of Shock Curvature on the Behavior of Hypersonic Boundary Layer, Polytechnic Institute of Brooklyn, Department of Aeronautical Engineering and Applied Mechanics, PIBAL Report No. 542, February 1960.

3. Love, A Reexamination of the Use of Simple Concepts for Predicting the Shape and Location of Detached Shock Waves, NACA TN 4170, December 1957.

4. Hammitt, A. G., "The Hypersonic Viscous Effect on a Flat Plate with Finite Leading Edge," Journal of Fluid Mechanics, Vol. 5, part 2, February 1959.

5. Thwaites, B., "Approximate Calculation of the Laminar Boundary Layer," Aeronautical Quarterly, Vol. 1, November 1949.

6. Rott and Crabtree, "Simplified Boundary Layer Calculations for Bodies of Revolution and for Yawed Wings," Journal of the Aeronautical Sciences, Vol. 19, No. 8, August 1952.

7. Illingworth, C. R., "Steady Flow in the Laminar Boundary Layer of a Gas," Proc. Roy. Soc. of London, Vol. 199, pp. 533-558, 1949.

8. Schlichting, Lecture Series "Boundary Layer Theory," Part I - Laminar Flows, NACA Tech. Memo No. 1217, April 1949.

9. Hayes and Probstein, Hypersonic Flow Theory, Academic Press, 1959.

10. Ames Research Staff, "Equations, Tables and Charts for Compressible Flow," NACA Report 1135, 1953.

11. Smith, A. M., "Improved Solutions of the Faulkner and Skan Boundary Layer Equation," IAS-SME Fund Paper No. FF-10, March 1954.

12. Martin and Reissner, Elementary Differential Equations, Addison Wesley, 1957.

13. Hildebrand, F. B., Introduction to Numerical Analysis, McGraw-Hill, 1956.